SIAM J. APPL. MATH.
Vol. 83, No. 2, pp. 576–602

RESOURCE-MEDIATED COMPETITION BETWEEN TWO PLANT SPECIES WITH DIFFERENT RATES OF WATER INTAKE*

CHUNYI GAI† AND THEODORE KOLOKOLNIKOV†

Abstract. We propose an extension of the well-known Klausmeier model of vegetation to two plant species that consume water at different rates. Rather than competing directly, the plants compete through their intake of water, which is a shared resource between them. In semiarid regions, the Klausmeier model produces vegetation spot patterns. We are interested in how the competition for water affects the coexistence and stability of patches of different plant species. We consider two plant types—a "thirsty" species and a "frugal" species—that only differ by the amount of water they consume per unit growth, while being identical in other aspects. We find that there is a finite range of precipitation rate for which two species can coexist. Outside of that range (when the rate is either sufficiently low or high), the frugal species out-competes the thirsty species. As the precipitation rate is decreased, there is a sequence of stability thresholds such that thirsty plant patches are the first to die off, while the frugal spots remain resilient for longer. The pattern consisting of only frugal spots is the most resilient. The next most resilient pattern consists of all-thirsty patches, with the mixed pattern being less resilient than either of the homogeneous patterns. We also examine numerically what happens for very large precipitation rates. We find that for a sufficiently high rate, the frugal plant takes over the entire range, out-competing the thirsty plant.

Key words. species coexistence, stability analysis, Klausmeier model, resource-mediated competition, reaction-diffusion systems, pattern formation

MSC codes. 35B35, 35B36, 35B40, 35Q92

DOI. 10.1137/21M144623X

1. Introduction.

Competition for resources has long been regarded as one of the main mechanisms in structuring plant communities and natural selection [1, 2, 3]. Unlike animals, plants do not move, and as such their competition is primarily mediated indirectly via competition for resources rather than direct territorial competition. These resources mainly include light, nutrients, and water [4, 5, 6]. Nutrients and water take place mostly underground and are considered among the most important mechanisms [6, 7].

While many mathematical models have been developed to account for direct competition among animals, there are fewer models of resource-mediated competition, especially with spatially explicit components [4, 8, 9]. In this paper, we study a phenomenological model of plant competition that incorporates competition for resources and—critically—incorporating the spatial aspect of this competition.

Our model is an extension of the well-known Klausmeier vegetation model [10], which was successfully used to model vegetation cover in semiarid regions where water resources are limited. The sparsity of water induces an intraspecies competition and can lead to self-organized vegetation patterns such as vegetation patches and stripes [10, 11, 12, 13, 14, 15]. These patterns can be thought of as a transition state from full vegetation to a desert state [16, 17, 11, 18, 19, 15].

In recent years more attention has been focused on the study of the competition and coexistence of two vegetation species [9, 20, 21, 8]. For example, a two-species

* Received by the editors September 14, 2021; accepted for publication (in revised form) December 6, 2022; published electronically April 28, 2023.
https://doi.org/10.1137/21M144623X

† Department of Mathematics and Statistics, Dalhousie University, Halifax, NS, Canada (Chuni.Gai@dal.ca, tkolokol@gmail.com).

reaction-diffusion system based on the single-species Klausmeier model is proposed in [9], and detailed ecological intuition and derivation are provided. It is shown that with a direct interspecific competition term (which corresponds to the shading effect) included, the coexistence of two plant species can occur as a long transient state, and eventually transit to a stable one-species state. Moreover, the impact of local intraspecific competition other than competition for limited water resources on the coexistence patterns is studied in [21, 8].

In this paper, we look at the competition for water between two plant species with different water absorption rates in the water-limited regime, where the vegetation patches form. We are interested in how the competition for water affects the coexistence and stability of patches of different plant species. We consider two plant species—a "thirsty" species and a "frugal" species—that only differ by the amount of water they consume per unit growth, while being identical in all other aspects.

1.1. Model derivation. Our starting point is the following variant of the Klausmeier model on a one-dimensional domain $|x| \le L$ with no-flux boundary conditions, incorporating two plant species and water-mediated competition between them:

(1.1)

$$\partial_t u_1 = \overbrace{D_u \partial_{xx} u_1}^{\text{plant dispersal}} - \overbrace{\mu u_1}^{\text{plant mortality}} + \overbrace{d_1 u_1 \left(c_{11}u_1 + c_{12}u_2\right) v}^{\text{plant growth of } u_1},$$

$$\partial_t u_2 = \overbrace{D_u \partial_{xx} u_2}^{\text{plant dispersal}} - \overbrace{\mu u_2}^{\text{plant mortality}} + \overbrace{d_2 u_2 \left(c_{21}u_1 + c_{22}u_2\right) v}^{\text{plant growth of } u_2},$$

$$\tau \partial_t v = \underbrace{D_v \partial_{xx} v}_{\text{water diffusion}} + \underbrace{a}_{\text{rain fall}} - \underbrace{bv}_{\text{evaporation}} - \underbrace{u_1 \left(c_{11}u_1 + c_{12}u_2\right) v - u_2 \left(c_{21}u_1 + c_{22}u_2\right) v}_{\text{water uptake by plants}}.$$

Here, u_1 and u_2 represent plant densities of the two types of plants, and v denotes the concentration of the water in the soil. To understand how limited water resources affect competition between plant species u_1 and u_2, we will consider their dynamics to be identical, except for the amount of water consumed per unit growth. We take these dynamics as originally suggested by Klausmeier [10]. In the absence of water, the plants wither at a rate μ, and they "diffuse" through seed dispersal in proportion to the diffusion constant D_u. The plant growth is the product of water uptake $u_i(c_{i1}u_1 + c_{i2}u_2)v$ and the yield of plant biomass per unit of water consumed d_i $(i = 1, 2)$, in which $(c_{i1}u_1 + c_{i2}u_2)$ describes how the two plants contribute to the growth of plant u_i via water infiltration feedback. The parameters c_{i1}, c_{i2} account for the different contributions to the water intake of the plant species u_i. The water diffuses through the soil according to the diffusion constant D_v. The parameter τ represents the differing timescales in changes in water level (in days, say) versus those in plant density (in months). Water is supplied by precipitation at rate a and is lost due to evaporation at rate bv.

Here is our justification for modifying the plant growth term in (1.1). In the classical Klausmeier model with a single plant species [10], the plant growth term is $\boldsymbol{u} \cdot uv$, where the first u represents positive water infiltration feedback induced by vegetation. However, when there are two plant species, the presence of the other plant species (say, u_2) helps increase water infiltration but may not contribute to the plant growth of its competitor (say, u_1). In this case, more water available in soil via

increased water infiltration does not guarantee more water available for each species. In fact, each species in multispecies plant communities often has a negative effect upon the other species' growth due to competition for the common water resource (see, e.g., [22, 23, 24] and references therein). To qualitatively describe the effect of the second plant species in (1.1), we modify the infiltration feedback term to $c_{i1}u_1 + c_{i2}u_2$, where $c_{11}, c_{22} > 0$, while c_{12}, c_{21} could be any sign.

First, by rescaling, we reduce (1.1) to the following nondimensional form (see derivation in Appendix A):

$$
\begin{aligned}
\partial_t u_1 &= \varepsilon^2 \partial_{xx} u_1 - u_1 + u_1 \left(u_1 + \frac{c_{12}}{c_{11}} u_2 \right) v, \\
\partial_t u_2 &= \varepsilon^2 \partial_{xx} u_2 - u_2 + \frac{d_2 c_{22}}{d_1 c_{11}} u_2 \left(\frac{c_{21}}{c_{22}} u_1 + u_2 \right) v, \\
\tau \partial_t v &= D \partial_{xx} v + a - bv - \frac{u_1^2 v}{\varepsilon} - \frac{c_{22}}{c_{11}} \frac{u_2^2 v}{\varepsilon} - \frac{c_{12} + c_{21}}{c_{11}} \frac{u_1 u_2 v}{\varepsilon}.
\end{aligned} \tag{1.2}
$$

A key assumption we make to obtain (1.2) is that $D_u \ll D_v$, because it is natural to assume that the "diffusion" of plants through seed dispersal is on a much slower scale than the water diffusion through the soil. Different regimes of D_u, D_v could model this assumption; in fact, a few parameter estimates for D_u in previous studies show that D_u could range from $10^{-6}\mathrm{m}^2/\mathrm{day}$ [9, 25] to $10^{-3}\mathrm{m}^2/\mathrm{day}$ [10]. In this paper, we are interested in the regime that $D_u = \mathcal{O}(\varepsilon^2)$, where $\varepsilon \ll 1$, and $D \equiv \frac{\varepsilon^2}{D_u} D_v = \mathcal{O}(1)$.

In terms of the original parameters, $\hat{a}, \hat{b}$ in (1.2) (hats are dropped; see Appendix A) are scaled with $\hat{a} = \frac{d_1 c_{11}}{\sqrt{\varepsilon \mu^3 c_{11}}} a$ and $\hat{b} = \frac{b}{\mu}$. According to the realistic parameter values that are valid for grass in semiarid regions reported in [9, 10], in which $\mu = 1.8, d_1 = 100, c_{11} = 0.003$, we assume that $\mu, d_i c_{ii}$ $(i = 1, 2) = \mathcal{O}(1)$. This scaling shows that $\hat{b} \ll \hat{a}$ in the limit $\varepsilon \to 0$. For simplicity, we assume $\hat{b}$ is sufficiently small and can be ignored in the system (but see Figure 9 (right) and the discussion in section 5, where the effect of increasing evaporation rate b is explored through numerical simulations).

The parameters $c_{ij} (i, j = 1, 2)$ correspond to different contributions of the presence of species u_j to water uptake of species u_i. Different scenarios can happen, depending on the choice of c_{ij}. When $c_{12}, c_{21} > 0$ and are on the same scale of c_{11}, c_{22}, u_1 and u_2 collaborate and promote the growth of each other. This is because the presence of one plant species helps water infiltrate in their areas more than absorbing soil water, hence increasing the water intake rate of the other plant species. This scenario is considered in [9], where the authors take $c_{21} = c_{11}, c_{22} = c_{21}$, representing identical water infiltration for both species. In this work, we explore an alternative scenario, where the presence of one plant species increases water infiltration capacity but does not help the water intake of the other plant species due to their competition for the water resource. This scenario corresponds to c_{12}, c_{21} very small compared to c_{11}, c_{22}, so the cross terms can be ignored due to the small ratio between c_{12}, c_{21} and c_{11}, c_{22}. Both scenarios are able to have coexistence of plant patterns; see Figures 1 and 2, which show the formation of plant patterns as obtained from full simulations of system (1.1) by FlexPDE [26]. In Figure 1, we take $c_{12} = c_{21} = 0$ so that the cross term $u_1 u_2 v$ is ignored; then two types of spikes are formed, and they do not occupy the same location. The behavior gets more complicated in the "collaboration" case. In Figure 2, we take the same initial conditions for u_1, u_2 and the same parameter values as in Figure 1 except $c_{12} = c_{11} = 1, c_{21} = c_{22} = 0.5$. For this parameter set, the steady state contains overlapped spikes.

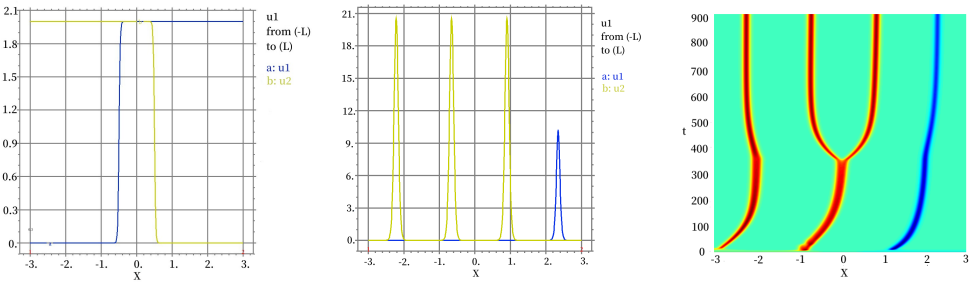

(a) u_1, u_2 at $t = 0$ (b) u_1, u_2 at $t = 10^5$ (c) Space-time plot of u_1,u_2

FIG. 1. (a), (b): *Plot of numerical solution u_1, u_2 of system* (1.1) *at different times with initial condition* $u_1 = 1 + \tanh(\frac{x+0.5}{\varepsilon}), u_2 = 1 - \tanh(\frac{x-0.5}{\varepsilon}), v = 3$, *which leads to the spike pattern shown in* (b). *The parameter values are* $D_u = 0.03^2, D_v = 1, c_{12} = c_{21} = 0, c_{11} = 1, c_{22} = 0.5, d_1 = 1, d_2 = 2, \mu = 1, a = 1, b = 0, L = 3$. (c): *Space-time plot of u_1 ("thirsty," in blue) and u_2 ("frugal," in red). Two types of spikes arise and slowly drift to their equilibrium locations.*

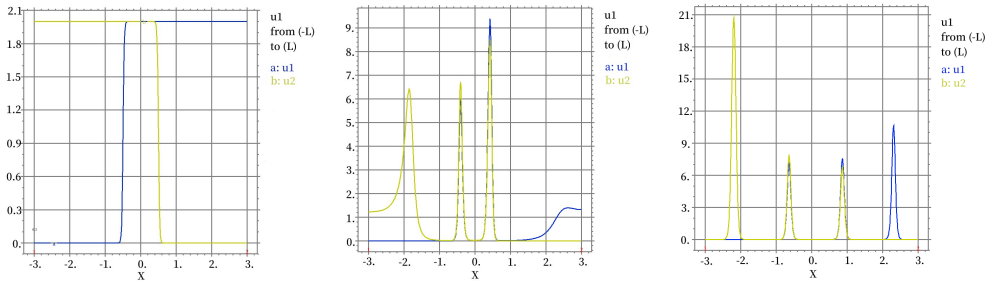

(a) u_1, u_2 at $t = 0$ (b) u_1, u_2 at $t = 7$ (c) u_1, u_2 at $t = 10^5$

FIG. 2. *Plot of numerical solution u_1, u_2 of system* (1.1) *at different times. The initial conditions are* $u_1 = 1 + \tanh(\frac{x+0.5}{\varepsilon}), u_2 = 1 - \tanh(\frac{x-0.5}{\varepsilon}), v = 3$, *which leads to the spike pattern shown in* (c). *The parameter values are* $D_u = 0.03^2, D_v = 1, c_{11} = c_{12} = 1, c_{21} = c_{22} = 0.5, d_1 = 1, d_2 = 2, \mu = 1, a = 1, b = 0, L = 3$.

In this paper, we focus on the water competition scenario between two plant species, i.e., we assume the ratios $\frac{c_{12}}{c_{11}}, \frac{c_{21}}{c_{11}}, \frac{c_{21}}{c_{22}} \ll 1$. Then system (1.2) can be simplified as follows:

$$
\begin{aligned}
\partial_t u_1 &= \varepsilon^2 \partial_{xx} u_1 - u_1 + u_1^2 v, \\
\partial_t u_2 &= \varepsilon^2 \partial_{xx} u_2 - u_2 + \frac{c_2 d_2}{c_1 d_1} u_2^2 v, \\
\tau \partial_t v &= D \partial_{xx} v + a - \frac{u_1^2 v}{\varepsilon} - \frac{c_2}{c_1} \frac{u_2^2 v}{\varepsilon},
\end{aligned}
\tag{1.3}
$$

where we write $c_1 = c_{11}, c_2 = c_{22}$. To simplify more parameters, we define the ratio of water intake rates $\beta \equiv \frac{c_2}{c_1}$ and define the plant growth rate as γ. Since plant growth is proportional to both the infiltration capability c_i that contributes water intake as well as the water-to-biomass conversion rate d_i, we then set $\gamma = c_1 d_1 = c_2 d_2$ to reflect the fact that the two plant species grow at the same rate with different water intake rates c_1, c_2. Then we obtain the system

$$
\begin{aligned}
\partial_t u_1 &= \varepsilon^2 \partial_{xx} u_1 - u_1 + u_1^2 v, \\
\partial_t u_2 &= \varepsilon^2 \partial_{xx} u_2 - u_2 + u_2^2 v, \\
\tau \partial_t v &= D \partial_{xx} v + a - \frac{u_1^2 v}{\varepsilon} - \beta \frac{u_2^2 v}{\varepsilon},
\end{aligned} \tag{1.4}
$$

which we will refer to as the "two-species vegetation model," and it satisfies no-flux boundary conditions $u_{1x} = u_{2x} = v_x = 0$ at $x = \pm L$.

The parameter τ represents the differing timescales in changes in water level (in days, say) versus those in plant density (in months); we assume τ is sufficiently small that the term $\tau \partial_t v$ does not affect the dynamics and can be discarded to leading order. For simplicity, we take $\tau = 0$, and note that this assumption can be replaced with "$\tau \ll D$" without any change in the results.

The ratio β indicates how thirsty is plant species u_1 compared to u_2. When $\beta < 1$, the species u_2 consumes less water than u_1, and the opposite is true when $\beta > 1$. Without loss of generality, we may also assume that $0 < \beta \leq 1$, so that u_1 is more thirsty (per unit growth) than u_2: u_1 is the "thirsty" species, whereas u_2 is the "frugal" species in such a case.

When $\beta = 1$, the two species are indistinguishable from each other, and the model (1.4) *behaves* like the "classical" Schnakenberg model [27, 28],

$$
\partial_t u = \varepsilon^2 \partial_{xx} u - u + u^2 v, \qquad \tau \partial_t v = D \partial_{xx} v + a - \frac{u^2 v}{\varepsilon}, \tag{1.5}
$$

where $u = u_1 + u_2$ (this model is itself a special case of the Klausmeier model).

1.2. Main results. It is well documented that the Schnakenberg model (1.5) admits spot solutions having N concentrations in u [28, 27]. More generally, similar results for spike-stability analysis are obtained in singularly perturbed two-component reaction-diffusion systems such as the Schnakenberg model, the Gierer–Meinhardt model [29, 30], and the Gray–Scott model [31, 32, 33, 34]. However, there are important differences both in the analysis and in the stability results for the 3-component system (1.4) when $\beta \neq 1$.

The two-species model (1.4) inherits spike solutions from (1.5) but has a much richer structure. Indeed, given any two nonnegative integers k_1, k_2, there exists a solution with a total $N = k_1 + k_2$ spikes corresponding to k_1 spikes in u_1 and k_2 spikes in u_2. We shall refer to this as a (k_1, k_2) pattern. In this paper, we will focus on the study of (k_1, k_2) spike solutions, which correspond to coexistent vegetation patches in different types in the singularly perturbed system (1.4); see Figure 3 for some examples. In particular, we are interested in how precipitation affects the behavior of the localized spike patterns.

At first glance, given N spikes, there is a total of 2^N possible ways to choose their type (each spike can be either u_1 or u_2 type). One might then think that there is a total of 2^N possible patterns with different spike heights and radii. However, it turns out that the spike *ordering* of spots does not affect spike profiles: only the total number of each type matters. This is because the maximum value of v between any two consecutive spikes (no matter whether they are of the same or different type) must be equal due to continuity, while u_1 and u_2 are exponentially small away from the spikes. As such, spikes of different types can be "glued" together into a single pattern using translation invariance with any ordering. This is illustrated in Figure 3, which shows two distinct orderings for the same number of parameters and number of spikes. Both orderings, however, have the same height and profile for the spikes

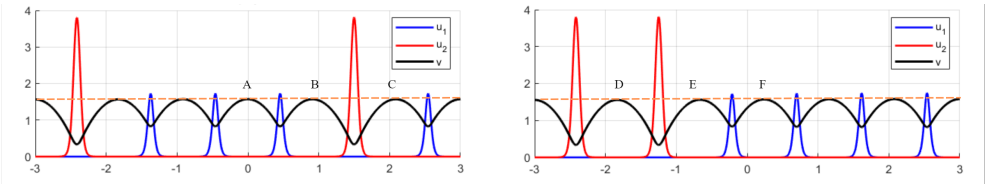

FIG. 3. *Two steady states of* (1.4)*, consisting of* $k_1 = 4$ *spikes of type* u_1 *(blue) and* $k_2 = 2$ *spikes of type* u_2 *(red). Parameters are* $\varepsilon = 0.025, a = 8, L = 3, D = 1, \beta = 0.5$*. The spike heights and profiles are the same for each type, regardless of the spike ordering. The local maxima of* v *are seen to be identical, as indicated by the dashed horizontal line.*

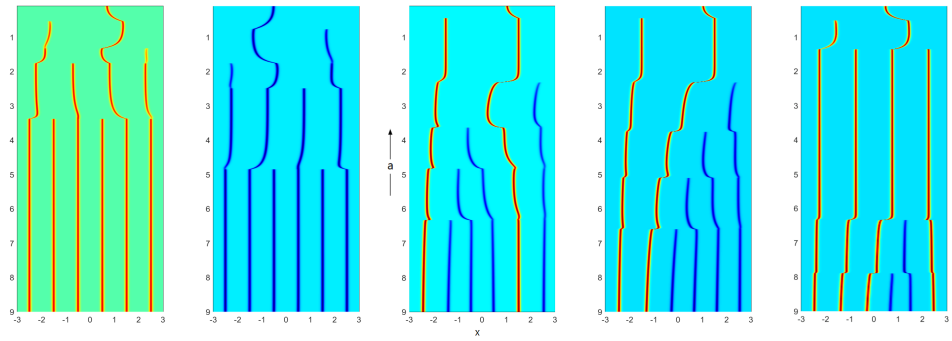

FIG. 4. *Spike death as* a *is decreased. Here,* $a = 10 - 10^{-5}t$ *and other parameters are* $\beta = 0.5$*,* $L = 3, D = 1, \varepsilon = 0.025$*. Color plot of* u_1 *("thirsty," in blue) and* u_2 *("frugal," in red) is shown as a function of* a*. The subpanels only differ in initial conditions and are arranged from most resilient pattern (on the left) to least resilient pattern (on the right). Note that a pattern of all-frugal patches is the most resilient, followed by all-thirsty, and then mixed patterns.*

u_1 and u_2. Note that all the local maxima of v in between the spikes have identical heights. The value of v at points A, B, C is the same and is equal to the value of v at D, E, F. At the same time, u_1, u_2 is exponentially small away from the spikes.

As such, there are only $N + 1$ patterns with distinct spike heights for fixed N, each corresponding to a different number of u_1-spikes (from zero to N). Note that although the spike ordering of spots has no effect on spike profiles, it can affect the large eigenvalue instability as shown in section 3.2.

In Figure 3, the "thirsty" patches are shown in blue and correspond to u_1, whereas the "frugal" patches are in red, corresponding to u_2. Note that the frugal plants have bigger height; this is because they absorb less water per unit growth, and hence there is more water remaining for them to grow more.

As rainfall rate a is decreased, competition of water between the plants triggers the collapse of one of the spikes in the overall pattern. This process is illustrated in Figure 4, which shows that as a is decreased, the *thirsty* spikes (in blue, corresponding to u_1) die out *first,* until only "frugal" (u_2, in red) remains. Our main goal is to study the stability of these N-spike equilibria. In particular, we derive the corresponding eigenvalue problem and consider both the small eigenvalues of order $\mathcal{O}(\varepsilon^2)$ and large eigenvalues of order $\mathcal{O}(1)$.

We now illustrate our main results. There are three thresholds that can affect the existence and stability of (k_1, k_2) spike patterns. One is the large eigenvalue threshold

TABLE 1

Instability thresholds a_f, a_s, and $\max(a_l)$ in N-spike patterns with $N = 5, 6$. The critical values are maximum in each column, which are the competition instability threshold a^* that triggers the collapse of one spike in the overall pattern. The parameters are $L = 3, \beta = 0.5, D = 1$.

5-spike patterns / thresholds	(4,1)	(3,2)	(2,3)	(1,4)
a_s	4.3372	4.9778	5.6471	2.3655
$\max(a_l)$	4.1362	4.7233	5.4138	DNE
a_f	2.3894	4.1053	5.3282	6.2754

6-spike patterns / thresholds	(5,1)	(4,2)	(3,3)	(2,4)	(1,5)
a_s	5.5649	6.2585	6.9725	7.7247	3.1677
$\max(a_l)$	5.3832	6.0649	6.7470	7.4579	DNE
a_f	2.6816	4.7327	6.2608	7.4492	8.4342

a_l such that the large eigenvalue becomes unstable as a decreases below a_l. The other two thresholds are small eigenvalue thresholds associated with either intraspecific competition (i.e., competition within u_1 or u_2 type) or interspecific competition (i.e., competition between u_1 and u_2 type). The interspecific competition threshold is denoted by the fold point a_f, and the intraspecific competition threshold is denoted by a_s. The maximum of these three critical values gives the competition instability threshold a^*, which triggers the collapse of plant patches. By comparing a_l, a_f, and a_s, we find that a_s is the dominant instability threshold for almost all (k_1, k_2) patterns, except the case where only one *thirsty* spike exists (i.e., $(1, N-1)$ patterns with $\beta < 1$ and $(N-1, 1)$ patterns with $\beta > 1$) and the dominant instability threshold is a_f. This result is illustrated in Table 1, where the three thresholds a_f, a_s, and a_l for different (k_1, k_2) patterns are computed. The large eigenvalue threshold a_l is *dependent* on spike orderings, while the other two are not. Therefore a_f, a_s are unique for each pattern, while a_l is different for different spike orderings. In Table 1, we compute the maximum of a_l and compare it with other thresholds in all types of 5-spike patterns and 6-spike patterns, and it can be seen that the instability threshold a^* (maximum in each column) is given by either a_s or a_f. Note that the large eigenvalue threshold may not exist under the given parameter values, such as the $(1, 4)$ pattern in Table 1, which means the $(1, 4)$ pattern is always stable with respect to the large eigenvalues.

For fixed N, we compared instability threshold a^* for different (k_1, k_2) spike patterns and found that the frugal species is more competitive. For example, if $\beta < 1$ (i.e., $c_2 < c_1$), then u_2 is more competitive, and one u_1-type spike will die out when bifurcation happens unless the pattern only contains u_2-type spikes. Otherwise, u_1 is more competitive, and one u_2-type spike will get killed when bifurcation occurs. Moreover, among the $N + 1$ combinations of spike patterns, homogeneous spike patterns (i.e., $(0, N)$ pattern or $(N, 0)$ pattern) are more resilient than mixed-spike patterns. These results are shown in Table 2, where the instability thresholds in terms of a are given for each (k_1, k_2) pattern. A smaller threshold a^* suggests that the corresponding pattern is more stable. As we see in Table 2, the 2nd row is the minimum in each column, which indicates that for fixed N, $(0, N)$ is the most stable pattern given that $\beta < 1$. Moreover, for mixed N-spike patterns, the more "frugal" spikes are contained, the more unstable the pattern is.

The setup of this paper is as follows. We construct the N-spike equilibria of the system (1.4) in section 2. In section 3 we analyze the stability of the N-spike equilibrium with respect to the large eigenvalues by deriving the corresponding nonlocal

TABLE 2

Theoretical predictions for competition instability thresholds a^* with parameters $L = 3, \beta = 0.5, D = 1$. The critical values in the first row indicate the most stable patterns in each column, while the critical values in the second row correspond to most unstable patterns. See also Figure 4 for comparison with numerics.

$a^*_{(k_1,k_2)}$ k_1 \ N	2	3	4	5	6
0	0.67	1.22	1.89	2.64	3.46
1	1.20	2.63	4.33	6.28	8.43
2	0.94	2.21	3.80	5.65	7.72
3		1.73	3.22	4.98	6.98
4			2.67	4.34	6.26
5				3.73	5.56
6					4.90

eigenvalue problem (NLEP), as well as the small eigenvalues by looking at asymmetric branches. The stability analysis is very similar to [27, 28] but with some key differences. We then show that the instability due to small eigenvalues is the dominant instability. In section 4 we briefly discuss the implications of our findings. Finally, we use numerics to explore what happens in the high-precipitation regime of large a, and we conclude with some open questions in section 5.

2. Construction of N-spike solutions. In this section, we construct N-spike equilibria of system (1.4), which contains k_1 u_1-spikes and k_2 u_2-spikes ($k_1 + k_2 = N$). To do this, we apply a similar analysis in [27] for the construction of equilibrium solutions, and first construct a local canonical one-spike equilibrium solution on a finite domain $2l$. Since there are two types of spikes in the steady state as shown in Figure 3, we construct one u_1-spike and one u_2-spike, and then apply the "gluing" technique and translation invariance to build the patterns on the global domain $(-L, L)$. In such a way, the resulting equilibrium solution on $(-L, L)$ is C^1 continuous.

We first construct one u_1-spike equilibrium solution on the domain $(-l_1, l_1)$. Note that there is no u_2-spike on this domain, so the local one u_1-spike solution centered at $x = 0$ satisfies

$$\begin{aligned} &\varepsilon^2 \partial_{xx} u_1 - u_1 + u_1^2 v = 0, \quad -l_1 < x < l_1, \\ &D\partial_{xx} v + a - \frac{u_1^2 v}{\varepsilon} = 0, \quad -l_1 < x < l_1, \\ &u_{1x}(\pm l_1) = v_x(\pm l_1) = 0. \end{aligned} \tag{2.1}$$

Now we apply the method of matched asymptotic expansions to construct the solutions. We first look at the inner region, where we introduce an inner variable

$$y = \frac{x}{\varepsilon}.$$

After collecting leading order terms we have

$$\begin{aligned} &u_{1yy} - u_1 + u_1^2 v = 0, \quad -\infty < y < \infty, \\ &v_{yy} = 0, \quad -\infty < y < \infty. \end{aligned} \tag{2.2}$$

We first solve the v equation in system (2.2). In order to match an outer solution, we require that v be bounded as $|y| \to \infty$. In this way, we obtain that v is a constant

independent of y in the inner region. Then solving the u_1 equation in system (2.2) yields

$$u_1 = \frac{1}{v_1} w\left(\frac{x}{\varepsilon}\right), \tag{2.3}$$

in which $v_1 = v(0)$ and $w(y)$ is the "ground state" profile satisfying

$$w'' - w + w^2 = 0, \quad w'(0) = 0, \quad w(y) > 0, \quad w(y) \to 0 \text{ as } |y| \to \infty; \tag{2.4}$$

it has a well-known explicit solution:

$$w(y) = \frac{3}{2}\operatorname{sech}^2\left(\frac{y}{2}\right). \tag{2.5}$$

In the outer region, defined away from $\mathcal{O}(\varepsilon)$ regions near $x = 0$, since $\varepsilon \ll 1$, u_1 is localized, and the terms $\frac{u_1^2 v}{\varepsilon}$ can be asymptotically approximated as a multiple of Dirac delta functions centered at $x = 0$. Therefore, v satisfies

$$D v_{xx} + a = \frac{6}{v_1}\delta(x), \quad v_x(\pm l_1) = 0. \tag{2.6}$$

Here we have used the fact that $\int_{0^-}^{0^+} \frac{u_1^2 v}{\varepsilon} dx = \int_{-\infty}^{\infty} u_1^2 v_1 dy = \frac{6}{v_1}$, where $(0^-, 0^+)$ is defined as a small interval that is slightly larger than the inner region. Integrating equation (2.6) over the domain $(-l_1, l_1)$ and imposing Neumann boundary conditions, we obtain that

$$v_1 = \frac{3}{a l_1}, \tag{2.7}$$

in which l_1 is to be determined. We then solve (2.6) by introducing Green's function $G(x; l_1)$ and let

$$v(x) = \bar{v} + \frac{6}{v_1} G(x; l_1) \tag{2.8}$$

for some constant $\bar{v}$ to be determined. Here $G(x; l_1)$ satisfies

$$D G_{xx}(x; l_1) + \frac{1}{2l_1} = \delta(x), \quad G_x(\pm l_1; l_1) = 0, \quad \int_{-l_1}^{l_1} G(x; l_1) dx = 0, \tag{2.9}$$

which has the solution

$$G(x; l_1) = -\frac{1}{4 D l_1} x^2 + \frac{1}{2D}|x| - \frac{l_1}{6D}. \tag{2.10}$$

The constant $\bar{v}$ is then determined by the matching condition $v(0) = v_1$:

$$\bar{v} = v_1 - \frac{6}{v_1} G(0; l_1) = v_1 + \frac{l_1}{D v_1}. \tag{2.11}$$

The same calculations apply to the construction on one u_2-spike on domain $(-l_2, l_2)$, where the local one u_2-spike solution centered at $x = 0$ satisfies

$$\begin{aligned} &\varepsilon^2 \partial_{xx} u_2 - u_2 + u_2^2 v = 0, \quad -l_2 < x < l_2, \\ &D \partial_{xx} V + a - \beta \frac{u_2^2 V}{\varepsilon} = 0, \quad -l_2 < x < l_2, \\ &u_{2x}(\pm l_2) = V_x(\pm l_2) = 0. \end{aligned} \tag{2.12}$$

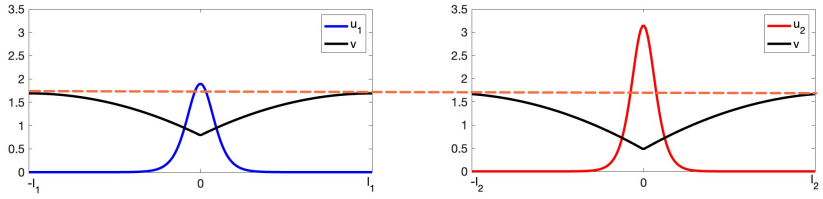

FIG. 5. *An example of single u_1 and u_2 spike constructed on $(-l_1, l_1)$ and $(-l_2, l_2)$, separately.*

Here we use $V(x)$ to distinguish from the solution $v(x)$ that corresponds to the u_1-spike. Solving system (2.12) using matched asymptotic expansions, we get

$$\text{inner solution: } u_2 = \frac{1}{V_2} w\left(\frac{x}{\varepsilon}\right), V_2 \equiv V(0) = \frac{3\beta}{a l_2}, \tag{2.13}$$

$$\text{outer solution: } V(x) = \tilde{V} + \frac{6\beta}{V_2} G(x; l_2), \tag{2.14}$$

where w and $G(x; l_2)$ are given in (2.5) and (2.10), respectively. $\tilde{V}$ is a constant that can be determined by the matching condition $V_2 = V(0)$:

$$\tilde{V} = V_2 - \frac{6\beta}{V_2} G(0; l_2) = V_2 + \frac{\beta l_2}{D V_2}. \tag{2.15}$$

We now construct an N-spike equilibrium solution on $(-L, L)$ with k_1 u_1-type spikes and k_2 u_2-type spikes. To do so, we use translation invariance and the matching condition that $v(l_1) = V(l_2)$ so that $v(x)$ is C^1 continuous on the global domain $(-L, L)$. This yields the length constraint

$$2k_1 l_1 + 2k_2 l_2 = 2L. \tag{2.16}$$

It remains to find the radius of the spikes l_1, l_2. For the global patterns that only contain u_1-type or u_2-type spikes (i.e., $(0, N)$ or $(N, 0)$ pattern), it is easy to see that $l_1 = l_2 = \frac{L}{N}$. For mixed-spike cases, we evaluate by imposing the continuity of v: $v(l_1) = V(l_2)$ (see Figure 5 for an example), and we obtain

$$\bar{v} - \tilde{V} = \frac{\beta l_2}{2 D V_2} - \frac{l_1}{2 D v_1}. \tag{2.17}$$

Then, subtracting (2.15) from (2.11), we get

$$\bar{v} - \tilde{V} = v_1 - V_2 - \frac{\beta l_2}{D V_2} + \frac{l_1}{D v_1}. \tag{2.18}$$

Combining the two equations (2.17) and (2.18) yields

$$v_1 - V_2 = \frac{3}{2D}\left(\frac{\beta l_2}{V_2} - \frac{l_1}{v_1}\right).$$

Then we eliminate v_1, V_2, l_1 using the fact that $v_1 = \frac{3}{a l_1}, V_2 = \frac{3\beta}{a l_2}$ and the length constraint (2.16), we obtain the following polynomial of l_2:

$$f(l_2) = e l_2^4 + p l_2^3 + q l_2^2 + r l_2 + s = 0, \tag{2.19a}$$

where

(2.19b)

$$e=(k_1^2-k_2^2), p=3Lk_2-\frac{k_1^2L}{k_2}, q=-3L^2, r=\frac{6D\beta k_1^2}{a^2}+\frac{6Dk_1^3}{a^2k_2}+\frac{L^3}{k_2}, s=-\frac{6D\beta Lk_1^2}{a^2k_2},$$

and once l_2 is solved through (2.19), l_1, v_1, V_2 can be determined, and the global pattern on $(-L, L)$ can be constructed by gluing the u_1 or u_2 types of spikes in the order as we wish.

In the end, we describe the equilibrium solution $u_1 = u_{1e}, u_2 = u_{2e}, v = v_e$ on $(-L, L)$. Near the jth spike, we have $u_{1e} = \frac{1}{v_1} w\left(\frac{x-x_j}{\varepsilon}\right)$ or $u_{2e} = \frac{1}{v_2} w\left(\frac{x-x_j}{\varepsilon}\right)$, depending on the type of jth spike, where x_j is the center of the jth spike and can be expressed as follows: $x_1 = -L + l_1$ if the first spike is u_1 type or $x_1 = -L + l_2$ if the first spike is u_2 type, and for $j = 1, 2, \ldots, N-1$,

$$x_{j+1} = \begin{cases} x_j + 2l_1 & \text{if the } j+1\text{th and } j\text{th spike are both } u_1 \text{ type,} \\ x_j + l_1 + l_2 & \text{if the } j+1\text{th and } j\text{th spike are different type,} \\ x_j + 2l_2 & \text{if the } j+1\text{th and } j\text{th spike are both } u_2 \text{ type.} \end{cases} \tag{2.20}$$

Then the equilibrium solution v_e satisfies

$$Dv_{xx} + a = \frac{6}{v_1}\sum_{j=1}^{k_1}\delta(x-x_j) + \frac{6\beta}{V_2}\sum_{j=k_1+1}^{N}\delta(x-x_j), v_x(\pm L) = 0, \tag{2.21}$$

and the solution to (2.21) is then readily represented in terms of an appropriate Green's function. We summarize our results as follows.

Result 2.1. *In the limit $\varepsilon \to 0$, system (1.4) has an N-spike equilibrium solution that contains k_1 u_1-type spikes and k_2 u_2-type spikes, in which $k_1 \geq 0$, $k_2 = N - k_1$:*

$$u_{1e}(x) = \sum_{j=1}^{k_1}\frac{w\left(\frac{x-x_j}{\varepsilon}\right)}{v_1}, \tag{2.22a}$$

$$u_{2e}(x) = \sum_{j=k_1+1}^{N}\frac{w\left(\frac{x-x_j}{\varepsilon}\right)}{V_2}, \tag{2.22b}$$

$$v_e(x) = v_0 + \frac{6}{v_1}\sum_{j=1}^{k_1}G(x;x_j) + \frac{6\beta}{V_2}\sum_{j=k_1+1}^{N}G(x;x_j). \tag{2.22c}$$

Here $w(y) = \frac{3}{2}\mathrm{sech}^2\left(\frac{y}{2}\right)$, $v_1 = \frac{3}{al_1}, V_2 = \frac{3\beta}{al_2}$, and x_j are given in (2.20), in which l_2 can be evaluated through (2.19) and $l_1 = \frac{L-k_2l_2}{k_1}$. $G(x;x_j)$ satisfies

$$DG_{xx}(x;x_j) + \frac{1}{2L} = \delta(x-x_j), \quad G_x(\pm L;x_j) = 0, \quad \int_{-L}^{L}G(x;x_j)dx = 0, \tag{2.23}$$

and it has the following solution:

$$G(x;x_j) = -\frac{1}{4DL}(x^2+x_j^2) + \frac{1}{2D}|x-x_j| - \frac{L}{6D}, \quad j = 1, \ldots, N. \tag{2.24}$$

The constant v_0 is then determined by the matching condition $v(x_i) = v_1$ (suppose the ith spike is u_1 type):

$$v_0 = v_1 - \frac{6}{v_1}\sum_{j=1}^{k_1}G(x_i;x_j) - \frac{6\beta}{V_2}\sum_{j=k_1+1}^{N}G(x_i;x_j). \tag{2.25}$$

2.1. Fold point of N-spike equilibrium. The N-spike equilibrium has a fold point $a_f(k_1, k_2)$, corresponding to the double root of the polynomial (2.19) (also referred to as the discriminant of the polynomial). It can be obtained by solving a polynomial system

$$f(l_2) = 0, f'(l_2) = 0.$$

We used Maple's groebner basis package to derive the following expression for the fold point:

(2.26)
$$\begin{aligned}\Delta(a) = &-256e^3s^3 + 192e^2prs^2 + 128e^2q^2s^2 - 144e^2qr^2s + 27e^2r^4\\ &- 144ep^2qs^2 + 6ep^2r^2s + 80epq^2rs\\ &- 18epqr^3 - 16eq^4s + 4eq^3r^2 + 27p^4s^2 - 18p^3qrs + 4p^3r^3 + 4p^2q^3s - p^2q^2r^2,\end{aligned}$$

where e, p, q, r, s are given in (2.19). Then $a_f(k_1, k_2)$ can be obtained by solving $\Delta(a_f(k_1, k_2)) = 0$ numerically.

Note that (2.19) is a fourth order polynomial when $k_1 \neq k_2$. When $k_1 = k_2$, it becomes a cubic polynomial and the discriminant (2.26) simplifies to

$$\Delta(a) = 27p^4s^2 - 18p^3qrs + 4p^3r^3 + 4p^2q^3s - p^2q^2r^2. \tag{2.27}$$

Moreover, when $\beta = 1$, (2.18) can be factored as

$$\begin{aligned}\Delta(a) = &\frac{34992k_1^6}{a^8k_2^6}\left(k_1^2k_2^2(k_1 - k_2)^2D^2 - \frac{2DNa^2L^3(k_1 - 2k_2)(k_1 - k_2/2)}{81} - \frac{L^6a^4}{972}\right)\\ &\times\left(DN^3 - \frac{L^3a^2}{3}\right)^2,\end{aligned}$$

which implies that $a_f = \sqrt{\frac{3DN^3}{L^3}}$. This result overlaps the critical value for competition instability for the case $\beta = 1$, which will be shown in section 3.1.

An example of a fold point with $k_1 = k_2 = 2$ is given in Figure 7. There are three solutions for $a > a_f$ and only one for $a < a_f$. By solving the full system (1.4) numerically, we observe that the second branch is stable when $a > a_f$; there are no stable solutions for $a < a_f$. As a consequence, the fold point a_f corresponds to one instability threshold of the system. Note that in the classical vegetation model which corresponds to our model when $\beta = 1$, the radius is unique, which is $l_1 = l_2 = \frac{L}{N}$. This matches our result shown in the right panel of Figure 7, where as $\beta = 1$, both the radius l_2 and l_1 equal $\frac{L}{2} = 0.75$.

3. Stability analysis. In this section, we analyze the stability of N-spike patterns constructed in section 2. Section 2.1 shows that there are three or four branches (depending on whether $k_1 = k_2$ or not) corresponding to different equilibria. In this paper we only consider and compute stability thresholds of the stable branch, such as the middle branch in Figure 7. We will first compute the bifurcation point where an asymmetric pattern bifurcates from the symmetric branch of the u_1- or u_2-spike. This threshold characterizes the stability threshold of N spike equilibria with respect to the small eigenvalues with $\lambda \to 0$ as $\varepsilon \to 0$. We will then derive a nonlocal eigenvalue problem (NLEP) which determines the stability of large eigenvalue ($\mathcal{O}(1)$). Note that the large eigenvalue threshold can be affected by the order of spikes, so in this section we consider spike steady state in general orderings. Numerical simulations are used to validate our stability results.

3.1. Asymmetric branches and competition instability thresholds. The primary mechanism that drives spike instability in one-dimensional reaction-diffusion models corresponds to a small-eigenvalue bifurcation [27, 28, 35]. The computation of small eigenvalues for the Schnakenberg model was done in [28], which shows that for a symmetric k-spike equilibrium solution, the small eigenvalues are all real and negative below the bifurcation point. Above the bifurcation point, $k-1$ small eigenvalues cross zero and the symmetric k-spike equilibrium becomes unstable. Instead of computing the small eigenvalues fully by deriving the eigenvalue problem, it was shown in [27] that this bifurcation point (at which there is a zero small eigenvalue) is characterized precisely by the emergence of an asymmetric solution (e.g., two spikes of unequal height) off the symmetric branch (i.e., spikes of equal height). In our two-species system, there are two types of spikes in the equilibrium solution. As expected, our two-species system inherits a similar structure, except that it has two such bifurcation points: one for each type of species, which we denote by a_{s1}, a_{s2}. By taking the maximum of the two, we will obtain the bifurcation threshold $a_s = \max(a_{s1}, a_{s2})$, which is responsible for the destabilization of the (k_1, k_2) pattern.

The key to computing a_{s1}, a_{s2} is to compute the value of v where $v' = 0$. These points occur in between any two consecutive spikes (the two consecutive spikes can be of the same type or different types). From (2.8) we have

$$\begin{aligned} v(x_j + l_1) &= g(l_1) = \frac{al_1^2}{2D} + \frac{3}{al_1}, \quad \text{when } x_j \text{ is the center of } u_1, \\ v(x_j + l_2) &= h(l_2) = \frac{al_2^2}{2D} + \frac{3\beta}{al_2}, \quad \text{when } x_j \text{ is the center of } u_2. \end{aligned} \tag{3.1}$$

Since the steady state $v(x)$ is continuous at the point in between two consecutive spikes of different types, and noting that each spike is symmetric about its center $x = x_j$, we have $v(x_j + l_1) = v(x_{j+1} - l_2) = v(x_{j+1} + l_2)$ (where the ordering is u_1-type spike on the left of u_2-type spike) or $v(x_j + l_2) = v(x_{j+1} - l_1) = v(x_{j+1} + l_1)$ (where the ordering is u_2-type spike on the left of u_1-type spike). This yields the following equation:

$$\frac{al_1^2}{2D} + \frac{3}{al_1} = \frac{al_2^2}{2D} + \frac{3\beta}{al_2}. \tag{3.2}$$

The function $g(l_1)$ has a unique global minimum point at l_{1c}, and it satisfies $g'(l_1) < 0$ on $(0, l_{1c})$ and $g'(l_1) > 0$ on (l_{1c}, ∞). Hence above the minimum point, there exist l_1 and $\hat{l}_1$ such that $g(l_1) = g(\hat{l}_1)$, and we can construct asymmetric spike solutions with the two different spike radii (see more details in [27, 36]). Such solutions exist for $l_1 < l_{1c} < \hat{l}_1$, and the same applies to $h(l_2)$. Therefore the bifurcation point corresponds to minimum points in (3.1). This is given by setting $\frac{\partial}{\partial l_1}\left(\frac{al_1^2}{2D} + \frac{3}{al_1}\right) = 0$ or $\frac{\partial}{\partial l_2}\left(\frac{al_2^2}{2D} + \frac{3\beta}{al_2}\right) = 0$ for a_{s1} and a_{s2}, respectively, which yields

$$a_{s1} = \sqrt{\frac{3D}{l_1^3}}, \tag{3.3}$$

$$a_{s2} = \sqrt{\frac{3\beta D}{l_2^3}}. \tag{3.4}$$

To calculate a_{s1}, we plug (3.3) into (3.2) and replace l_2 by $\frac{L - k_1 l_1}{k_2}$ from (2.1); this yields the following cubic polynomial in terms of l_1:

$$(k_1^3 - 3k_1k_2^2 - 2\beta k_2^3)l_1^3 + 3L(k_2^2 - k_1^2)l_1^2 + 3k_1L^2l_1 - L^3 = 0. \tag{3.5}$$

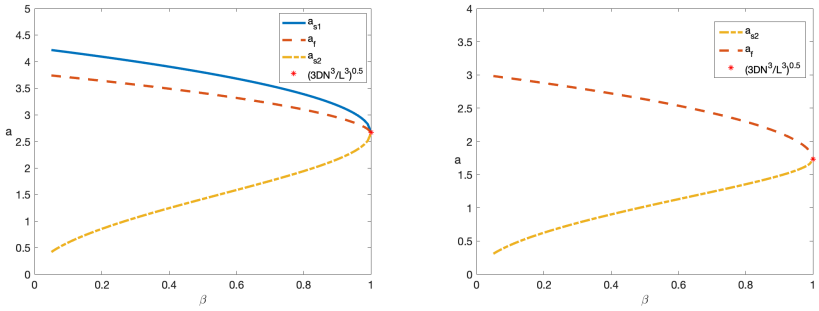

FIG. 6. *Plot of three thresholds* a_f (2.27), a_{s1} (3.3), *and* a_{s2} (3.4) *versus* β *for a* $(2,2)$ *spike pattern (left panel) and a* $(1,2)$ *spike pattern (right panel). In the left figure (*$(2,2)$ *pattern),* $a_s = a_{s1}$ *is the dominant instability threshold, while in the right figure (for* $(1,2)$ *pattern), there is no competition within the* u_1*-spike, so only* a_{s2} *exist and* $a_{s2} < a_f$*; thus* a_f *is the dominant instability threshold. Here the parameters are* $D = 1, L = 3$.

We then can get the value of a_{s1} by solving this polynomial for l_1 and plugging it back into (3.3). The value for a_{s2} in (3.4) can be calculated in the same way.

These two critical values (3.3), (3.4) suggest that as a decreases below a_{s1} (or a_{s2}), asymmetric patterns in u_1 (or u_2) type appear. This is analogous to the classical Schnakenberg model, where asymmetric patterns are proved to be unstable [27], and the corresponding unstable eigenfunction introduces competition between the spikes. Therefore, one of the spikes is annihilated in finite time when competition instability occurs. Here in the case of two species, the bifurcation threshold $a_s = \max(a_{s1}, a_{s2})$. Suppose that $\beta < 1$; then $l_1 < l_2$ (this claim is proved in Appendix B), and it follows that $a_{s1} > a_{s2}$. Thus $a_s = a_{s1}$, which implies that the spike annihilation within the u_1-type spike happens first. Similarly, we get $a_s = a_{s2}$ when $\beta > 1$. For the case $\beta = 1$, we have $l_1 = l_2 = \frac{L}{N}$ so that $a_s = a_{s1} = a_{s2} = \sqrt{\frac{3DN^3}{L^3}}$. This recovers the threshold previously obtained in [27, 28] for the classical Schnakenberg model. The above computations require that there be at least two spikes of type u_1 (or u_2) (which guarantees the existence of intraspecific competition within u_1 and u_2). In summary, we obtain

$$a_s = \begin{cases} \sqrt{\frac{3D}{l_1^3}}, & k_1 \geq 2 \text{ with either (a) } \beta < 1 \text{ and } k_2 \text{ is arbitrary} \\ & \text{or (b) } \beta > 1 \text{ and } k_2 = 1, \\ \sqrt{\frac{3\beta D}{l_2^3}}, & k_2 \geq 2 \text{ with either (c) } \beta > 1 \text{ and } k_1 \text{ is arbitrary} \\ & \text{or (d) } \beta < 1 \text{ and } k_1 = 1. \end{cases} \tag{3.6}$$

Note that the threshold (3.6) computes the competition within the same type of spikes, and it does not cover the competition between u_1- and u_2-spikes. Therefore, this result does not work for the $(1,1)$ pattern. However, as we compare a_s and a_f obtained in section 2.1, we find that $a_f < a_s$ in the cases (a), (c) shown in (3.6) and $a_f = a_s = \sqrt{\frac{3DN^3}{L^3}}$ when $\beta = 1$. This is shown in Figure 6, where we compared a_f and a_s for $(2,2)$ and $(1,2)$ patterns. We conjecture that a_f is another small eigenvalue threshold that corresponds to interspecific competition between u_1- and u_2-spikes.

There exist two special cases (case (b), (d) in (3.6)): either $k_1 = 1$ (i.e., $(1, N-1)$ spike patterns) with $\beta < 1$, or $k_2 = 1$ (i.e., $(N-1, 1)$ spike patterns) with $\beta > 1$. For these cases, $a_s < a_f$, so the dominant instability is triggered by the fold point a_f as

computed in section 2 instead of a_s. This is illustrated in Figure 6, where in the left panel ($(2,2)$ pattern) $a_s = a_{s1} > a_f$, and the dominant threshold is a_s, while in the right panel ($(1,2)$ pattern) $a_f > a_s = a_{s2}$, so the dominant threshold is a_f. This is further illustrated in Figure 4, which shows an excellent agreement between numerics and theoretical results. For example, the last panel in Figure 4 shows that the first spike death is caused by $a_s = 7.7247$ in a $(2,4)$ pattern, and the second spike death is caused by $a_f = 6.2754$ in a $(1,4)$ pattern. The theoretical thresholds a_s and a_f can be found in Table 1.

3.2. Large eigenvalues and nonlocal eigenvalue problem. In this section we compute the large $\mathcal{O}(1)$ eigenvalues by deriving the corresponding eigenvalue problem. We start by linearizing around the steady state given in (2.22). That is, we let $u_1 = u_{1e} + e^{\lambda t}\varphi_1, u_2 = u_{2e} + e^{\lambda t}\varphi_2$, and $v = v_e + e^{\lambda t}\xi$. Note that here the (k_1, k_2) spike steady states are considered in general spike orderings without changing the profile of u_1 and u_2. Upon substituting into (1.4) and assuming that $|\varphi_1| \ll 1, |\varphi_2| \ll 1, |\xi| \ll 1$ we obtain the following eigenvalue problem:

$$\lambda\varphi_1 = \varepsilon^2\varphi_{1xx} - \varphi_1 + 2u_{1e}v_e\varphi_1 + u_{1e}^2\xi, \quad \varphi_{1x}(\pm L) = 0, \tag{3.7a}$$

$$\lambda\varphi_2 = \varepsilon^2\varphi_{2xx} - \varphi_2 + 2u_{2e}v_e\varphi_2 + u_{2e}^2\xi, \quad \varphi_{2x}(\pm L) = 0, \tag{3.7b}$$

$$\tau\lambda\xi = D\xi_{xx} - \frac{1}{\varepsilon}\left[2u_{1e}v_e\varphi_1 + 2\beta u_{2e}v_e\varphi_2 + \left(u_{1e}^2 + \beta u_{2e}^2\right)\xi\right], \quad \xi_x(\pm L) = 0. \tag{3.7c}$$

Near the jth spike, we change variables $x = x_j + \varepsilon y$. To leading order, we obtain $\xi(y) \sim \xi_j := \xi(x_j)$, and in the inner region we have

$$\lambda\varphi \sim \varphi_{yy} - \varphi + 2w\varphi + \frac{w^2}{v(x_j)^2}\xi_j, \tag{3.8}$$

where

$$\varphi = \begin{cases} \varphi_1, & j\text{th spike is } u_1 \text{ type}, \\ \varphi_2, & j\text{th spike is } u_2 \text{ type}, \end{cases} \qquad v(x_j) = \begin{cases} v_1, & j\text{th spike is } u_1 \text{ type}, \\ v_2, & j\text{th spike is } u_2 \text{ type}. \end{cases}$$

Due to localization of the coefficients in (3.8), we look for an eigenfunction for (3.8) in the form

$$\varphi \sim \sum_{j=1}^{N} \Phi_j\left(\frac{x - x_j}{\varepsilon}\right),$$

where $\Phi_j(y) \to 0$ as $|y| \to \infty$. In the outer region, both φ_1 and φ_2 are assumed to be localized functions, so ξ satisfies

$$\xi_{xx} - \mu^2\xi = \sum_{j=1}^{N} c_j\delta(x - x_j), \quad \xi_x(\pm L) = 0, \tag{3.9}$$

where $\mu = \sqrt{\frac{\tau\lambda}{D}}$ and c_j is defined as

$$c_j = \begin{cases} \frac{1}{D}\left(2\int_{-\infty}^{\infty} w(y)\Phi_j(y)dy + \frac{6}{v_1^2}\xi_j\right), & j\text{th spike is } u_1 \text{ type}, \\ \frac{\beta}{D}\left(2\int_{-\infty}^{\infty} w(y)\Phi_j(y)dy + \frac{6}{v_2^2}\xi_j\right), & j\text{th spike is } u_2 \text{ type}. \end{cases} \tag{3.10}$$

We first solve (3.9) and write $\xi(x)$ as

$$\xi = \sum_{j=1}^{N} c_j G^{(\mu)}(x; x_j), \tag{3.11}$$

where $G^{(\mu)}(x;x_j)$ satisfies

$$G^{(\mu)}_{xx}(x;x_j)-\mu^2 G^{(\mu)}(x;x_j)=\delta(x-x_j),\quad G^{(\mu)}_x(\pm L;x_j)=0. \tag{3.12}$$

Solving (3.12) yields

$$G^{(\mu)}(x;x_j)=-\frac{1}{\mu\sinh(2\mu L)}\begin{cases}\cosh\left(\mu(x+L)\right)\cosh\left(\mu(x_j-L)\right), & x<x_j,\\ \cosh\left(\mu(x_j+L)\right)\cosh\left(\mu(x-L)\right), & x>x_j.\end{cases} \tag{3.13}$$

Evaluating (3.11) at $x=x_j$, we obtain that

$$\xi(x_i)=\xi_i=\sum_{j=1}^{N}c_j G^{(\mu)}_{i,j},$$

where $G^{(\mu)}_{i,j}=G^{(\mu)}(x_i;x_j)$ given in (3.13). In matrix form, it can be written as

$$\vec{\xi}=\mathcal{G}^{(\mu)}\mathcal{B}\left(\frac{2}{D}\int w\vec{\Phi}dy+\frac{6}{D}\mathcal{V}\vec{\xi}\right), \tag{3.14}$$

where

(3.15)

$$\vec{\Phi}\equiv\begin{pmatrix}\Phi_1\\ \vdots\\ \Phi_N\end{pmatrix},\quad \vec{\xi}\equiv\begin{pmatrix}\xi_1\\ \vdots\\ \xi_N\end{pmatrix},\quad \text{and}\quad \mathcal{G}^{(\mu)}\equiv\begin{pmatrix}G^{(\mu)}_{1,1} & G^{(\mu)}_{1,2} & \cdots & G^{(\mu)}_{1,N}\\ G^{(\mu)}_{2,1} & \ddots & \cdots & G^{(\mu)}_{2,N}\\ \vdots & \vdots & \ddots & \vdots\\ G^{(\mu)}_{N,1} & G^{(\mu)}_{N,2} & \cdots & G^{(\mu)}_{N,N}\end{pmatrix},$$

and $\mathcal{B}$ and $\mathcal{V}$ are diagonal matrices with

(3.16)

$$\mathcal{B}_{j,j}=\begin{cases}1, & j\text{th spike is } u_1 \text{ type},\\ \beta, & j\text{th spike is } u_2 \text{ type},\end{cases}\qquad \text{and}\quad \mathcal{V}_{j,j}=\begin{cases}\frac{1}{v_1^2}, & j\text{th spike is } u_1 \text{ type},\\ \frac{1}{v_2^2}, & j\text{th spike is } u_2 \text{ type}.\end{cases}$$

Solving system (3.14) we get

$$\vec{\xi}=\frac{2}{D}\left(\mathcal{I}-\frac{6}{D}\mathcal{G}^{(\mu)}\mathcal{B}\mathcal{V}\right)^{-1}\mathcal{G}^{(\mu)}\mathcal{B}\int w\vec{\Phi}dy. \tag{3.17}$$

Note that at the jth spike, we can rewrite (3.8) as

$$\lambda\Phi_j=L_0\Phi_j+\frac{w^2}{v(x_j)^2}\xi_j, \tag{3.18}$$

where $L_0\Phi_j=\Phi_{jyy}-\Phi_j+2w\Phi_j$, and in matrix form we have

$$\lambda\vec{\Phi}=L_0\vec{\Phi}+\frac{w^2}{v(x_j)^2}\vec{\xi}. \tag{3.19}$$

Substituting (3.17) into (3.19), the resulting eigenvalue problem becomes

$$\lambda\vec{\Phi}=L_0\vec{\Phi}+M\frac{w^2\int w\vec{\Phi}dy}{\int w^2dy}, \tag{3.20}$$

where

$$M = \frac{2\int w^2 dy}{D}\mathcal{V}\left(\mathcal{I} - \frac{6}{D}\mathcal{G}^{(\mu)}\mathcal{B}\mathcal{V}\right)^{-1}\mathcal{G}^{(\mu)}\mathcal{B}. \tag{3.21}$$

The solution to (3.20) is $\vec{\Phi}(y) = \vec{m}\phi_0(y)$ as the eigenvalue problem is the same for each j given that $\vec{m}$ is the eigenvector for the matrix problem $M\vec{m} = \eta\vec{m}$. Then (3.20) becomes

$$\vec{m}\lambda\phi_0 = \vec{m}L_0\phi_0 + M\vec{m}\frac{w^2\int w\phi_0 dy}{\int w^2 dy}, \tag{3.22}$$

and this yields the following nonlocal eigenvalue problem:

$$\lambda\phi_0 = L_0\phi_0 + \eta w^2\frac{\int w\phi_0 dy}{\int w^2 dy}, \tag{3.23}$$

where η is the eigenvalue of M given in (3.21) and $\vec{m}$ is the corresponding eigenvector.

Note that when $\beta = 1$, u_1, u_2 are essentially the same, so that $l_1 = l_2 = \frac{L}{N}$ and $v_1 = v_2 = \frac{3N}{aL}$. Then matrix M in (3.21) becomes

$$M = \frac{2\int w^2}{Dv_1^2}\left(\mathcal{I} - \frac{6}{Dv_1^2}\mathcal{G}^{(\mu)}\right)^{-1}\mathcal{G}^{(\mu)}, \tag{3.24}$$

which recovers the results of large eigenvalues in the two-component Schnakenberg model [28].

For our system with $\beta \neq 1$, since it's hard to compute the general results for eigenvalues of M given in (3.21), here we consider a special case where there are 1 u_1-type and 1 u_2-type spikes. In this case we have

(3.25)

$$\begin{aligned} M &= \frac{2\int w^2}{D}\begin{pmatrix} \frac{1}{v_1^2} & 0 \\ 0 & \frac{1}{v_2^2} \end{pmatrix}\begin{pmatrix} 1 - \frac{6}{Dv_1^2}G_{1,1}^{(\mu)} & -\frac{6\beta}{Dv_2^2}G_{1,2}^{(\mu)} \\ -\frac{6}{Dv_1^2}G_{2,1}^{(\mu)} & 1 - \frac{6\beta}{Dv_2^2}G_{2,2}^{(\mu)} \end{pmatrix}^{-1}\begin{pmatrix} G_{1,1}^{(\mu)} & \beta G_{1,2}^{(\mu)} \\ G_{2,1}^{(\mu)} & \beta G_{2,2}^{(\mu)} \end{pmatrix} \\ &= C\begin{pmatrix} Dv_2^2 G_{1,1}^{(\mu)} - 6\beta\det(\mathcal{G}) & Dv_2^2\beta G_{1,2}^{(\mu)} \\ Dv_1^2 G_{2,1}^{(\mu)} & Dv_1^2\beta G_{2,2}^{(\mu)} - 6\beta\det(\mathcal{G}) \end{pmatrix}, \end{aligned}$$

where $\mathcal{G} = \begin{pmatrix} G_{1,1}^{(\mu)} & G_{1,2}^{(\mu)} \\ G_{2,1}^{(\mu)} & G_{2,2}^{(\mu)} \end{pmatrix}$ and $C = \frac{2\int w^2}{D^2 v_1^2 v_2^2 - 6\beta D v_1^2 G_{2,2}^{(\mu)} - 6D v_2^2 G_{1,1}^{(\mu)} + 36\beta\det(\mathcal{G})}$.

In the limit $\tau \to 0$, we have $\mu \to 0$, and after some algebra matrix M can be simplified as

$$M = \frac{-2}{\beta Dv_1^2 + Dv_2^2 + 6\beta L}\begin{pmatrix} Dv_2^2 + 6\beta L & \beta Dv_2^2 \\ Dv_1^2 & \beta Dv_1^2 + 6\beta L \end{pmatrix}. \tag{3.26}$$

Computing the eigenvalues of M, we obtain that

$$\eta_1 = -2, \eta_2 = \frac{-12\beta L}{\beta Dv_1^2 + Dv_2^2 + 6\beta L}. \tag{3.27}$$

Let's recall the following lemma from [29].

TABLE 3

Large eigenvalue instability thresholds a_l in different spike orderings. The parameters are $L = 3, \beta = 0.5, D = 1$. Note that in the seco2nd table we only show the spike orderings that have distinct thresholds.

a_l patterns / (k_1, k_2)	$(s\,s\,s\,l)$	$(s\,s\,l\,s)$	$(s\,l\,s\,s)$	$(l\,s\,s\,s)$
(3,1)	2.9898	2.7709	2.7709	2.9898

a_l patterns / (k_1, k_2)	$(s\,s\,s\,l\,l)$	$(s\,s\,l\,s\,l)$	$(s\,s\,l\,l\,s)$	$(s\,l\,s\,s\,l)$	$(s\,l\,s\,l\,s)$	$(l\,s\,s\,s\,l)$
(3,2)	4.7233	4.4944	4.4941	4.5941	4.1552	4.7656

LEMMA 3.1. *Consider the nonlocal eigenvalue problem*

$$\phi'' - \phi + 2w\phi - \alpha \frac{\int w\phi}{\int w^2} w^2 = \lambda\phi. \tag{3.28}$$

(1) *If $\alpha > 1$, then there exists a positive eigenvalue to* (3.28).
(2) *If $\alpha < 1$, then either $\lambda = 0$ with the eigenfunction $\phi = c_0 w'$ for some constant c_0 or*

$$Re(\lambda) < 0.$$

From Lemma 3.1, we see that the critical threshold for the stability of large eigenvalues is such that

$$-1 = \frac{-12\beta L}{\beta D v_1^2 + D v_2^2 + 6\beta L}. \tag{3.29}$$

Plugging in $v_1 = \frac{3}{a l_1}, v_2 = \frac{3\beta}{a l_2}$, we get the critical threshold for the stability of large eigenvalues (denoted as a_l):

$$a_l = \sqrt{\frac{3D}{2L}\left(\frac{1}{l_1^2} + \frac{\beta}{l_2^2}\right)}. \tag{3.30}$$

For the more general case $N \geq 3$, large eigenvalue threshold a_l corresponds to the value of a for which the largest eigenvalue of M equals -1. Table 3 shows the thresholds a_l for different spike orders in $(3,1)$ and $(3,2)$ spike patterns. Note that for different orders of spikes, a_l can be different; in Table 3 we denote the ordering of u_1 and u_2 as s, l. Although there are $\binom{N}{k_2}$ different spike orderings for fixed k_1, k_2, the number of instability thresholds is less than $\binom{N}{k_2}$ since the threshold is the same when ordering is just flipped (for example, see Table 3, which shows that the large eigenvalue threshold is the same for $(s\,s\,s\,l)$ and $(l\,s\,s\,s)$).

It is well known that for two-component reaction-diffusion systems the competition instability threshold in N-spike equilibria ($N \geq 2$) cross the threshold for small eigenvalues first [27, 28, 35]. And it appears to still be the case in the two-species vegetation system (1.4). We compare the instability thresholds a_l and a_s for (k_1, k_2) patterns numerically; the results are shown in Figure 7, where we tried different β for a $(2,2)$ spike pattern, and it is always the case $a_s > a_l$. As we increase β to 1, a_s overlaps with a_f, and a_l *does not exist* on the stable branch, which means the whole branch is stable to large eigenvalues. Similar results can be obtained for other

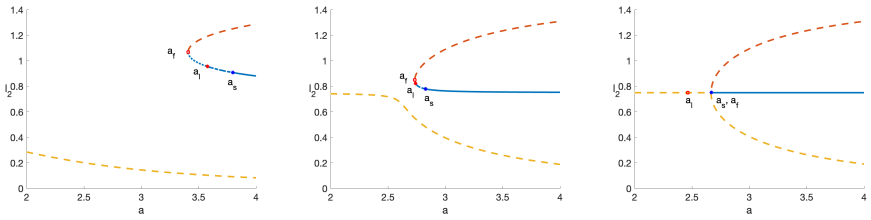

FIG. 7. *Radius of u_2-spike l_2 versus a for a $(2,2)$ spike pattern. The instability thresholds on the stable branch are shown. Solid lines: linearly stable for both the small eigenvalues and the large eigenvalues; dash-dotted lines: unstable for the small eigenvalues but stable for the large eigenvalues; dotted line: unstable for both small eigenvalues and large eigenvalue. Here we choose $\beta = 0.5, 0.99, 0.9999$ from left to right; the other parameters are $D = 1, L = 3$.*

patterns. See also Table 1 for more results on the comparison between a_l and a_s. We then conjecture that for arbitrary (k_1, k_2) patterns it is still the case that the competition instability threshold a_s crosses the threshold for small eigenvalues first.

We have $a_s > a_l$ and N-spike equilibria are stable with respect to both large and small eigenvalues when $a > a_s$; when $a_l < a < a_s$ they are stable with respect to large eigenvalues but unstable with respect to small eigenvalues; when $a < a_l$, N-spike equilibria become unstable with respect to both large and small eigenvalues.

We now combine these results with those in section 3.1. We have shown in Figure 6 that $a_s > a_f$ for $k_1 \geq 2$ ($\beta < 1$) or $k_2 \geq 2$ ($\beta > 1$) and $a_s < a_f$ for either $(1, N-1)$ spike patterns ($\beta < 1$) or $(N-1, 1)$ spike patterns ($\beta > 1$). For the former case, $a_f < a_l < a_s$, thus a_s is the dominant instability threshold; for the latter one, we found that a_l *does not exist* in the stable branch, and $a_f > a_s$ is the dominant instability threshold.

Therefore, there are $N+1$ distinct instability thresholds denoted as a^* for each N, each corresponding to a different number of u_1 spikes (from zero to N). Moreover, we are curious about stability ordering within these patterns. We compared a^* for different $(k_1, N-k_1)$ patterns with fixed N, and Table 1 illustrates the results for various patterns. This is further illustrated in Figure 4.

We now summarize the result as follows.

RESULT 3.2. *An N-spike steady state to system* (1.4) *which contains k_1 u_1-spikes and k_2 u_2-spikes becomes unstable when a decreases to $a^* = \max(a_f, a_s)$. Both a_f and a_s can be explicitly computed numerically: a_f is the largest real root of* (2.26) *and a_s can be obtained by solving the coupled system* (3.5) *and* (3.6). *Moreover, using (k_1, k_2) to represent different patterns regardless of the order of different spikes, where $k_1 = 0, \ldots, N$, $k_2 = N - k_1$, we compare a^* for different patterns which are shown in Table* 1 *and find that the stability of the patterns has the following order (from most stable to most unstable) depending on the ratio of water intake rate β:*

$$\beta < 1 : (0, N) > (N, 0) > (N-1, 1) > (N-2, 2) > \cdots > (1, N-1),$$
$$\beta > 1 : (N, 0) > (0, N) > (1, N-1) > (2, N-2) > \cdots > (N-1, 1).$$

It seems surprising that the spike pattern that contains only thirsty species is more stable than mixed patterns. This is because the thirsty patches in mixed patterns have a smaller size (or radius) than the pure thirsty vegetation pattern (see Appendix B for proof of this claim). Hence the thirsty patches in mixed patterns are less competitive and are more likely to die out. This can also be verified by the dominant competition threshold formula. Suppose $\beta < 1$, so l_1 is the radius of thirsty patches and $a_s = \sqrt{\frac{3D}{l_1^3}}$;

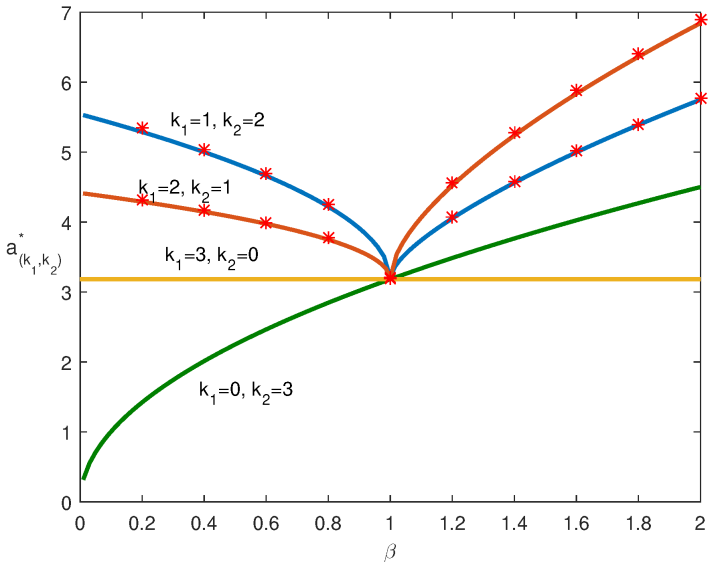

FIG. 8. *Instability regions for all possible combinations of* 3*-spike patterns. Below each line the corresponding* (k_1, k_2) *pattern becomes unstable and one* u_1*-type spike will get killed when* $k_1 \geq 1$ *or one* u_2*-type spike gets killed when* $k_1 = 0$*. The red dots are obtained from full simulations of system* (1.4)*. Here the parameters are* $L = 2, D = 1, \varepsilon = 0.03$*.*

then a smaller radius yields a larger competition threshold, which suggests that the corresponding pattern is more unstable.

Figure 8 shows stability regions for all possible combinations of 3-spike patterns. As a decreases below the critical line, the corresponding pattern becomes unstable. The colored lines are plotted using analytical results $a^* = \max(a_f, a_s)$, and the red dots are obtained from full simulations of system (1.4) by FlexPDE, in which we look for the numerical thresholds by gradually decreasing a until the pattern becomes unstable and one thirsty patch collapses. The numerical simulations are in full agreement with our analytical results.

4. Discussion. We have proposed a two-species model (corresponding to two different plants), with competition for a common resource (water). This model is based on the well-known Klausmeier model of vegetation patterns. For simplicity, we concentrated on two plant species that grow at the same rate but have different rates of water consumption: thirsty and frugal plants. We have shown that in the water-constrained regime where spike patterns exist, the two species can coexist. However, as the precipitation rate decreases, it eventually induces an interspecies competition between the thirsty plants, leading to the death of some of them. The "frugal" plants are initially unaffected by the water sparsity as long as the thirsty plants are still present, and thus can out-compete the more "thirsty" plant, leading to the death of thirsty plants and survival of the more frugal plant.

We found two distinct mechanisms which triggered the dominant instability, depending on the number of spikes for each type. When only one spike of the thirsty plant is present (represented in blue in Figure 4), the dominant instability corresponds to a fold point a_f as derived in section 2.1, and leads to the death of the blue spike when triggered. When more than one blue spike exists, the dominant instability corresponds to asymmetric spike bifurcation at a_s as explained in section 3.1. This leads

to competition instability among the blue spikes, with one of the blue spikes getting killed. In summary, no matter which mechanism triggers spike death, the blue spikes always get killed first until only red spikes remain. In either case, when $\beta = 1$ (so that the two species are indistinguishable), the instability thresholds correspond exactly to those derived for a symmetric N-spike configuration for the Schnakenberg model in [27, 28]. Note that in section 3.1 the conclusion that the dominant instability corresponds to asymmetric spike bifurcation at a_s rather than large eigenvalue instability threshold a_l is a conjecture. An interesting open problem is to prove it analytically.

There have been many studies on the competition and coexistence of several plant species [9, 20, 21, 8]. For example, [9] studies metastable coexistence patterns arising from one-species Turing-type patterns. Different from [9], where the coexistence patterns are unstable but can persist for a long time, we focus on the study of localized spike solutions, which correspond to coexistent vegetation patches in different types in water-limited regions. These multispike vegetation patterns are stable for appropriate parameters.

Studies on localized spike solutions for the Klausmeier model have been done; see [37], where an extended version of the Klausmeier model with nonconstant parameters is considered. In [37], similar techniques are applied to construct N-spike solutions, and the dynamical movements of spikes are studied by deriving the corresponding ODEs that describe the motion of each spike location. In our paper, instead of looking at the spike motions, we study the existence and stability of localized patterns. Moreover, our two-species vegetation model (1.4) exhibits a richer variety of localized spatiotemporal patterns compared to the singularly perturbed two-component reaction-diffusion systems.

5. Outlook. Numerous possible extensions and modifications of model (1.4) are possible for future study. For example, the water uptake can be periodic having "pulse phase" of water intake followed by "pulse interphase," where water uptake ceases; this can have a large effect on coexistence [38]. Another extension is to model the effects of light absorption separately from nutrients, which can lead to cooperation between different plant species that specialize in different ecological niches. For instance, in [39] the authors showed that mixed pine-oak forests can enhance each other due to differing light/nutrient requirements.

What happens as precipitation rate is increased? For the Schnakenberg model, it is well known that as a is increased, spot replication is observed [19, 35]. A further increase of a eventually leads to a uniform-vegetation state [15]. In the case of two species, self-replication is also observed for sufficiently large a; see Figure 9 (left), where the initial condition consists of two vegetation patches of different types and we choose a large precipitation rate $a = 25$. As we see in Figure 9 (left), as time goes on, the two species self-replicate to multispots and eventually coexist. However, depending on parameters, this can further lead to the more frugal plant species taking over the entire domain. See Figure 9 (center), where we increase precipitation rate a to 35; then self-replication occurs but eventually the frugal species takes over the entire domain. This suggests that the coexistence of two plant species occurs only for precipitation parameter $a \in (a_{\text{coexistence,min}}, a_{\text{coexistence,max}})$. It is an open question to determine the upper boundary of this interval.

In our analysis, we made a few simplifying assumptions on (1.1), such as discarding the evaporation rate b. Figure 9 (right) demonstrates numerically the effect of increasing the evaporation rate with the initial condition consisting of two thirsty and three frugal vegetation patches. As the evaporation increases and less water is available, the number of plant clusters decreases until eventually species extinction is

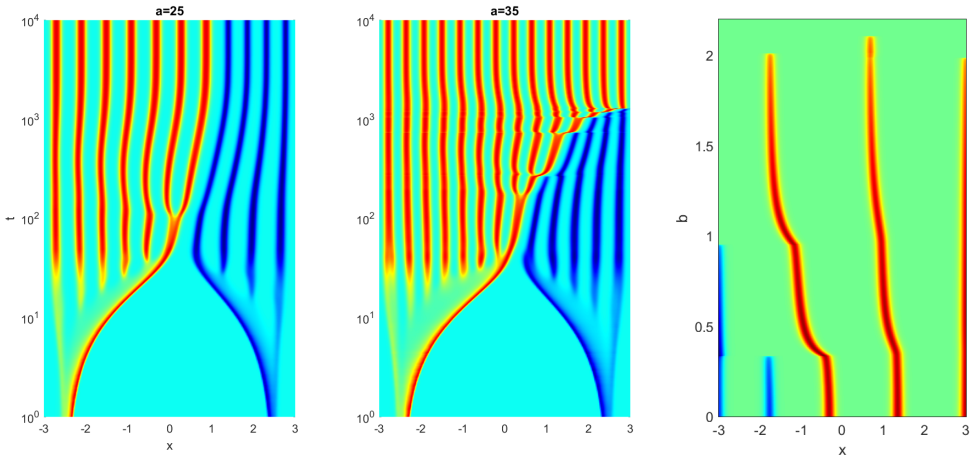

FIG. 9. *Left and center: Space-time plot of u_1 (blue) and u_2 (red) as a function of time with a as indicated and with $\beta = 0.6, \varepsilon = 0.03, D = 1, L = 3$. Initial conditions consist of two spots on opposite sides of the domain. Left: self-replication of both types of plants, leading to coexistence. Center: Self-replication is followed by a takeover of the entire domain by the red plant. Note that time is plotted on a log scale. Right: Space-time plot of u_1 (blue) and u_2 (red) under the effect of increasing evaporation. The initial condition consists of two thirsty spots and three frugal spots. The vertical scale corresponds to the evaporation rate b, which is being ramped up from zero according to the formula $b = 0.001t$. Here, the full model (1.1) is simulated with the following parameters: $D_u = 0.05^2, D_v = 1, \mu = 1, d_1 = 1.3,\ d_2 = 1,\ c_{11}u_1 + c_{12}u_2 = u_1,\ c_{21}u_1 + c_{22}u_2 = u_2,\ a = 2, L = 3$.*

observed. As expected, the thirsty plants tend to be killed off before the frugal plants. Studies on the classical Klausmeier model with evaporation term have been done previously. For example, the generalized Klausmeier–Gray–Scott model was considered in [40, 41], which shows the original Klausmeier model, restricted to flat ground but allowing the diffusion of biomass, is identical to the Gray–Scott model. It has been shown in [34] that symmetric spike equilibrium solution in the Gray–Scott model in the low feed rate regime has a saddle-node bifurcation point. So we conjecture that the evaporation term in our system can affect the fold point of the N-spike equilibrium solutions.

The behavior of the system is very different for even larger a, as shown in Figure 10. In this case, the two plants self-organize into a propagating wave of vegetation. The red wave (corresponding to a more frugal plant) eventually takes over the entire domain. Similar phenomenon can be observed in other competition kinetics [42]. An open problem is to compute the propagation speed as a function of system parameters.

Another interesting open problem is to consider general τ. In this paper, we have assumed τ is small enough that $\tau\partial_t v$ can be discarded to leading order. For more general cases where τ is sufficiently large, a Hopf bifurcation can happen. This phenomenon has been studied in singularly perturbed two-component reaction-diffusion systems such as the Gierer–Meinhardt model and Gray–Scott model [43, 44]. In our two-species system, two types of Hopf bifurcation can be observed numerically when τ is large. This is shown in Figure 11, in which Hopf bifurcation leading to oscillations in the spike amplitudes and in the spike motion is observed depending on different values of parameters.

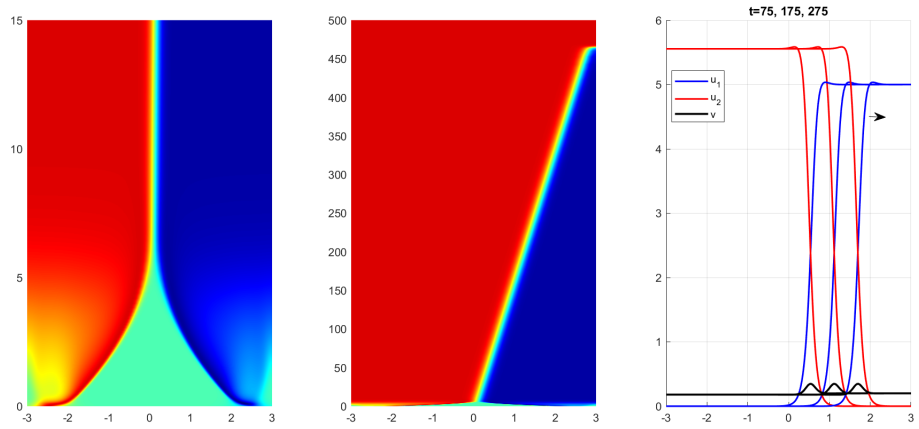

FIG. 10. *Space-time plot of u_1 (blue) and u_2 (red) as a function of time with $\varepsilon = 0.1, \beta = 0.9, a = 50$. Initial conditions consist of two spots on the opposite sides of the domain. Left: Initial space-filling dynamics for $t \in (0, 15)$. Middle: Takeover of the domain by the red plant, $t \in (0, 500)$. Snapshot of the propagating waves at three different times as indicated. The wave propagates at a constant speed.*

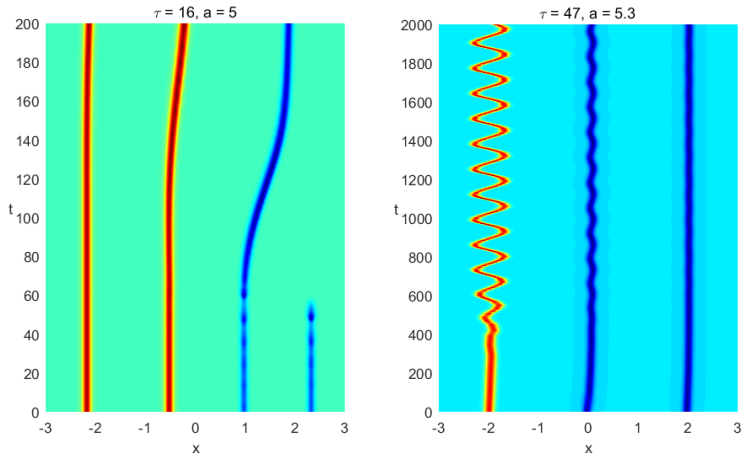

FIG. 11. *Space-time plot of u_1 (blue) and u_2 (red) as a function of time with τ and a as indicated and with $\beta = 0.5, \varepsilon = 0.03, D = 1, L = 3$. Left: Hopf bifurcation in spike amplitude, leading to one spike killed off. Right: Hopf bifurcation in spike motion of both u_1 and u_2 spike.*

The model demonstrates how biodiversity can be very sensitive to precipitation levels. It exhibits species coexistence in a "Goldilocks" region of precipitation rate $a \in (a_{\text{coexistence,min}}, a_{\text{coexistence,max}})$. For high precipitation when $a > a_{\text{coexistence,max}}$, the frugal species "pushes out" the thirsty species in an invasion-wave-type dynamics. For low precipitation $a < a_{\text{coexistence,min}}$, the thirsty species dies out through direct competition for water resources. This demonstrates the evidence of fragility of coexistence if the precipitation changes too much, e.g., as a consequence of climate change [45, 15].

The Klausmeier model is qualitative and phenomenological rather than quantitative and does not incorporate explicitly the exact biological details of water/nutrient uptake. Our goal was to use a sort of "minimal" model which nonetheless can exhibit realistic behavior. Despite its simplicity, the model exhibits a very rich and wide range of biologically viable scenarios, including coexistence for an intermediate range of precipitation levels, as well as the domination of more frugal plants when water levels are either too high or too low. The model suggests that for moderate water levels, initial conditions play an important role in determining coexistence versus domination (cf. Figure 4). In contrast, at high water levels, coexistence or domination is independent of initial conditions (cf. Figure 9), which is similar to Lotka–Volterra-type models [46].

Appendix A. In this appendix we derive nondimensionalization of system (1.1). First we scale the variables as follows:

$$\hat{x} = \frac{x}{x_0}, \quad \hat{t} = \frac{t}{t_0}, \quad \hat{u}_1 = \frac{u_1}{u_0}, \quad \hat{u}_2 = \frac{u_2}{u_0}, \quad \hat{v} = \frac{v}{v_0},$$

where x_0, t_0, u_0, v_0 are constant units that are to be determined. Plugging the nondimensional variables into (1.1), we get

(A.1)

$$\begin{aligned}
\hat{u}_{1\hat{t}} &= \frac{t_0}{x_0^2} D_u \partial_{\hat{x}\hat{x}} \hat{u}_1 - \mu t_0 \hat{u}_1 + d_1 c_{11} u_0 v_0 t_0 \hat{u}_1 \left(\hat{u}_1 + \frac{c_{12}}{c_{11}} \hat{u}_2 \right) \hat{v}, \\
\hat{u}_{2\hat{t}} &= \frac{t_0}{x_0^2} D_u \partial_{\hat{x}\hat{x}} \hat{u}_2 - \mu t_0 \hat{u}_2 + d_2 c_{22} u_0 v_0 t_0 \hat{u}_2 \left(\frac{c_{21}}{c_{22}} \hat{u}_1 + \hat{u}_2 \right) \hat{v}, \\
\tau \hat{v}_{\hat{t}} &= \frac{t_0}{x_0^2} D_v \partial_{\hat{x}\hat{x}} \hat{v} + \frac{t_0}{v_0} a - b t_0 \hat{v} - u_0^2 t_0 c_{11} \hat{u}_1 \left(\hat{u}_1 + \frac{c_{12}}{c_{11}} \hat{u}_2 \right) \hat{v} - u_0^2 t_0 c_{22} \hat{u}_2 \left(\frac{c_{21}}{c_{22}} \hat{u}_1 + \hat{u}_2 \right) \hat{v}.
\end{aligned}$$

According to a few parameter estimates for D_u in previous studies, in which D_u could range from $10^{-6}\mathrm{m}^2/\mathrm{day}$ [9, 25] to $10^{-3}\mathrm{m}^2/\mathrm{day}$ [10], here we consider the regime that $D_u = \mathcal{O}(\varepsilon^2)$, in which $\varepsilon \ll 1$, and $D_v = \mathcal{O}(1)$. This regime reflects the fact that the spread of plants is much slower than the diffusion of water [9, 47]. We then choose t_0 and x_0 such that $\mu t_0 = 1$, and $\frac{t_0}{x_0^2} D_u = \varepsilon^2$. Then system (A.1) becomes the following singularly perturbed reaction diffusion system:

(A.2)

$$\begin{aligned}
\hat{u}_{1\hat{t}} &= \varepsilon^2 \partial_{\hat{x}\hat{x}} \hat{u}_1 - \hat{u}_1 + \frac{d_1 c_{11} u_0 v_0}{\mu} \hat{u}_1 \left(\hat{u}_1 + \frac{c_{12}}{c_{11}} \hat{u}_2 \right) \hat{v}, \\
\hat{u}_{2\hat{t}} &= \varepsilon^2 \partial_{\hat{x}\hat{x}} \hat{u}_2 - \hat{u}_2 + \frac{d_2 c_{22} u_0 v_0}{\mu} \hat{u}_2 \left(\frac{c_{21}}{c_{22}} \hat{u}_1 + \hat{u}_2 \right) \hat{v}, \\
\tau \hat{v}_{\hat{t}} &= D \partial_{\hat{x}\hat{x}} \hat{v} + \frac{1}{\mu v_0} a - \frac{b}{\mu} \hat{v} - \frac{u_0^2 c_{11}}{\mu} \hat{u}_1 \left(\hat{u}_1 + \frac{c_{12}}{c_{11}} \hat{u}_2 \right) \hat{v} - \frac{u_0^2 c_{22}}{\mu} \hat{u}_2 \left(\frac{c_{21}}{c_{22}} \hat{u}_1 + \hat{u}_2 \right) \hat{v},
\end{aligned}$$

where $D \equiv \frac{\varepsilon^2}{D_u} D_v = \mathcal{O}(1)$. Similar to other singularly perturbed reaction-diffusion systems, (A.2) admits localized patterns. We scale the magnitude of the localized spike patterns to $\mathcal{O}(1)$ by taking $u_0 = \mathcal{O}(\frac{1}{\sqrt{\varepsilon}})$ and choosing u_0, v_0 such that $\frac{u_0^2 c_{11}}{\mu} = \frac{1}{\varepsilon}$ and $\frac{d_1 c_{11} u_0 v_0}{\mu} = 1$. This yields

$$u_0 = \sqrt{\frac{\mu}{\varepsilon c_{11}}}, \quad v_0 = \frac{\sqrt{\varepsilon \mu c_{11}}}{d_1 c_{11}},$$

and system (A.2) becomes

$$\begin{aligned}
\hat{u}_{1\hat{t}} &= \varepsilon^2 \partial_{\hat{x}\hat{x}} \hat{u}_1 - \hat{u}_1 + \hat{u}_1 \left(\hat{u}_1 + \frac{c_{12}}{c_{11}} \hat{u}_2 \right) \hat{v}, \\
\hat{u}_{2\hat{t}} &= \varepsilon^2 \partial_{\hat{x}\hat{x}} \hat{u}_2 - \hat{u}_2 + \frac{d_2 c_{22}}{d_1 c_{11}} \hat{u}_2 \left(\frac{c_{21}}{c_{22}} \hat{u}_1 + \hat{u}_2 \right) \hat{v}, \\
\tau \hat{v}_{\hat{t}} &= D \partial_{\hat{x}\hat{x}} \hat{v} + \frac{d_1 c_{11}}{\sqrt{\varepsilon \mu^3 c_{11}}} a - \frac{b}{\mu} \hat{v} - \frac{\hat{u}_1^2 \hat{v}}{\varepsilon} - \frac{c_{22}}{c_{11}} \frac{\hat{u}_2^2 \hat{v}}{\varepsilon} - \frac{c_{12} + c_{21}}{c_{11}} \frac{\hat{u}_1 \hat{u}_2 \hat{v}}{\varepsilon}.
\end{aligned} \tag{A.3}$$

In the end, we scale $\hat{a} = \frac{d_1 c_{11}}{\sqrt{\varepsilon \mu^3 c_{11}}} a$ and $\hat{b} = \frac{b}{\mu}$. Dropping the hats, we obtain system (1.2) as shown in section 1.1.

Appendix B. In this appendix we prove the radius of thirsty patches in mixed patterns is smaller than that of the spike in pure thirsty patterns.

Without loss of generality, we assume $\beta < 1$ so u_1 is the thirsty species. We denote the radii of the thirsty patches in mixed patterns as l_1 and the radii of the spikes in pure thirsty pattern as $\tilde{l}_1$ (the proof is the same for the case $\beta > 1$).

First, we show that in mixed-spike patterns the radius of thirsty patches is smaller than that of frugal patches, i.e., $l_1 < l_2$.

From (2.5), (2.7), we have the heights of the two types of spike:

$$u_1(x_j) = \frac{3}{2v_1} = \frac{a l_1}{2}, \tag{B.1}$$

$$u_2(x_j) = \frac{3}{2v_2} = \frac{a l_2}{2\beta}, \tag{B.2}$$

where x_j is the center of the u_1- or u_2-spike, depending on the spike locations of the two types. It is observed from simulations that frugal spikes are higher than thirsty spikes in the pattern (see Figure 3 for some examples). Therefore, $\frac{a l_1}{2} < \frac{a l_2}{2\beta}$ and it follows that

$$l_2 > \beta l_1. \tag{B.3}$$

Then, rewriting (3.2), we get

$$\frac{a}{2D}(l_1 + l_2)(l_1 - l_2) = \frac{3}{a l_1 l_2}(\beta l_1 - l_2) < 0, \tag{B.4}$$

which yields $l_1 < l_2$.

Then for mixed patterns where $k_1 \geq 1, k_2 \geq 1$, we have

$$L = k_1 l_1 + k_2 l_2 > k_1 l_1 + k_2 l_1 = (k_1 + k_2) l_1 = N l_1, \tag{B.5}$$

which yields

$$l_1 < \frac{L}{N} = \tilde{l}_1. \tag{B.6}$$

Therefore, the radius of thirsty patches in mixed patterns is smaller than that of the spike in pure thirsty pattern. Moreover, since the height of each spike is proportional to its radius, a smaller radius l_1 implies a smaller patch size.

Acknowledgments. We are grateful to Michael Ward for useful discussions. We thank the anonymous referees for extensive suggestions which helped to substantially improve the paper.

REFERENCES

[1] C. Van Der Waal, H. De Kroon, W. F. De Boer, I. M. A. Heitkönig, A. K. Skidmore, H. J. De Knegt, F. Van Langevelde, S. E. Van Wieren, R. C. Grant, B. R. Page et al., *Water and nutrients alter herbaceous competitive effects on tree seedlings in a semi-arid savanna*, J. Ecol., (2009), pp. 430–439.

[2] D. R. Gordon, J. M. Menke, and K. J. Rice, *Competition for soil water between annual plants and blue oak (Quercus douglasii) seedlings*, Oecologia, 79 (1989), pp. 533–541.

[3] M. Gioria and B. A. Osborne, *Resource competition in plant invasions: Emerging patterns and research needs*, Front. Plant Sci., 5 (2014), 501.

[4] J. M. Craine and R. Dybzinski, *Mechanisms of plant competition for nutrients, water and light*, Funct. Ecol., 27 (2013), pp. 833–840.

[5] E. T. Aschehoug, R. Brooker, D. Z. Atwater, J. L. Maron, and R. M. Callaway, *The mechanisms and consequences of interspecific competition among plants*, Ann. Rev. Ecol. Evol. Syst., 47 (2016), pp. 263–281.

[6] B. B. Casper and R. B. Jackson, *Plant competition underground*, Annu. Rev. Ecol. Syst., 28 (1997), pp. 545–570.

[7] F. Berendse, *Competition between plant populations at low and high nutrient supplies*, Oikos, 71 (1994), pp. 253–260.

[8] L. Eigentler, *Species coexistence in resource-limited patterned ecosystems is facilitated by the interplay of spatial self-organisation and intraspecific competition*, Oikos, 130 (2021), pp. 609–623.

[9] L. Eigentler and J. A. Sherratt, *Metastability as a coexistence mechanism in a model for dryland vegetation patterns*, Bull. Math. Biol., 81 (2019), pp. 2290–2322.

[10] C. A. Klausmeier, *Regular and irregular patterns in semiarid vegetation*, Science, 284 (1999), pp. 1826–1828.

[11] O. Lejeune, M. Tlidi, and P. Couteron, *Localized vegetation patches: A self-organized response to resource scarcity*, Phys. Rev. E, 66 (2002), 010901.

[12] R. Martínez-García, J. M. Calabrese, E. Hernández-García, and C. López, *Vegetation pattern formation in semiarid systems without facilitative mechanisms*, Geophys. Res. Lett., 40 (2013), pp. 6143–6147.

[13] F. Borgogno, P. D'Odorico, F. Laio, and L. Ridolfi, *Mathematical models of vegetation pattern formation in ecohydrology*, Rev. Geophys., 47 (2009), RG1005.

[14] K. Siteur, E. Siero, M. B. Eppinga, J. D. M. Rademacher, A. Doelman, and M. Rietkerk, *Beyond Turing: The response of patterned ecosystems to environmental change*, Ecol. Complex, 20 (2014), pp. 81–96.

[15] Y. Chen, T. Kolokolnikov, J. Tzou, and C. Gai, *Patterned vegetation, tipping points, and the rate of climate change*, European J. Appl. Math., 26 (2015), pp. 945–958.

[16] J. von Hardenberg, E. Meron, M. Shachak, and Y. Zarmi, *Diversity of vegetation patterns and desertification*, Phys. Rev. Lett., 87 (2001), 198101.

[17] Y. R. Zelnik, H. Uecker, U. Feudel, and E. Meron, *Desertification by front propagation?*, J. Theoret. Biol., 418 (2017), pp. 27–35.

[18] O. Lejeune, M. Tlidi, and R. Lefever, *Vegetation spots and stripes: Dissipative structures in arid landscapes*, Int. J. Quantum Chem., 98 (2004), pp. 261–271.

[19] K. Gowda, Y. Chen, S. Iams, and M. Silber, *Assessing the robustness of spatial pattern sequences in a dryland vegetation model*, Proc. R. Soc. A Math. Phys. Eng. Sci., 472 (2016), 20150893.

[20] L. Eigentler, *Species Coexistence in Vegetation Patterns Facilitated by the Interplay of Spatial Self-Organisation and Intraspecific Competition*, bioRxiv, preprint, 2020.

[21] L. Eigentler, *Intraspecific competition in models for vegetation patterns: Decrease in resilience to aridity and facilitation of species coexistence*, Ecol. Complex, 42 (2020), 100835.

[22] Q. Hou, J. Brandle, K. Hubbard, M. Schoeneberger, C. Nieto, and C. Francis, *Alteration of soil water content consequent to root-pruning at a windbreak/crop interface in Nebraska, USA*, Agrofor. Syst., 57 (2003), pp. 137–147.

[23] A. W. Miller and S. G. Pallardy, *Resource competition across the crop-tree interface in a maize-silver maple temperate alley cropping stand in Missouri*, Agrofor. Syst., 53 (2001), pp. 247–259.

[24] S. Jose, A. R. Gillespie, J. R. Seifert, D. B. Mengel, and P. E. Pope, *Defining competition vectors in a temperate alley cropping system in the midwestern USA:* 3. *Competition for nitrogen and litter decomposition dynamics*, Agrofor. Syst., 48 (2000), pp. 61–77.
[25] E. Gilad, J. von Hardenberg, A. Provenzale, M. Shachak, and E. Meron, *A mathematical model of plants as ecosystem engineers*, J. Theoret. Biol., 244 (2007), pp. 680–691.
[26] PDE Solutions Inc., https://www.pdesolutions.com/index.html.
[27] M. J. Ward and J. Wei, *The existence and stability of asymmetric spike patterns for the Schnakenberg model*, Stud. Appl. Math., 109 (2002), pp. 229–264.
[28] D. Iron, J. Wei, and M. Winter, *Stability analysis of Turing patterns generated by the Schnakenberg model*, J. Math. Biol., 49 (2004), pp. 358–390.
[29] J. Wei, *On single interior spike solutions of the Gierer-Meinhardt system: Uniqueness and spectrum estimates*, European J. Appl. Math., 10 (1999), pp. 353–378.
[30] D. Iron, M. J. Ward, and J. Wei, *The stability of spike solutions to the one-dimensional Gierer-Meinhardt model*, Phys. D, 150 (2001), pp. 25–62.
[31] A. Doelman, T. J. Kaper, and P. A. Zegeling, *Pattern formation in the one-dimensional Gray-Scott model*, Nonlinearity, 10 (1997), pp. 523–563.
[32] C. B. Muratov and V. V. Osipov, *Static spike autosolitons in the Gray-Scott model*, J. Phy. A, 33 (2000), pp. 8893–8916.
[33] C. B. Muratov and V. V. Osipov, *Stability of the static spike autosolitons in the Gray–Scott model*, SIAM J. Appl. Math., 62 (2002), pp. 1463–1487, https://doi.org/10.1137/S0036139901384285.
[34] T. Kolokolnikov, M. J. Ward, and J. Wei, *The existence and stability of spike equilibria in the one-dimensional Gray-Scott model: The low feed-rate regime*, Stud. Appl. Math., 115 (2005), pp. 21–71.
[35] T. Kolokolnikov and J. Wei, *Pattern formation in a reaction-diffusion system with space-dependent feed rate*, SIAM Rev., 60 (2018), pp. 626–645, https://doi.org/10.1137/17M1116027.
[36] T. Kolokolnikov, M. Ward, and J. Wei, *The Stability of Steady-State Hot-Spot Patterns for a Reaction-Diffusion Model of Urban Crime*, preprint, https://arxiv.org/abs/1201.3090, 2012.
[37] R. Bastiaansen and A. Doelman, *The dynamics of disappearing pulses in a singularly perturbed reaction-diffusion system with parameters that vary in time and space*, Phys. D, 388 (2019), pp. 45–72.
[38] S. Schwinning and C. K. Kelly, *Plant competition, temporal niches and implications for productivity and adaptability to climate change in water-limited environments*, Funct. Ecol., 27 (2013), pp. 886–897.
[39] T. Jucker, O. Bouriaud, D. Avacaritei, I. Dănilă, G. Duduman, F. Valladares, and D. A. Coomes, *Competition for light and water play contrasting roles in driving diversity-productivity relationships in Iberian forests*, J. Ecol., 102 (2014), pp. 1202–1213.
[40] S. van der Stelt, A. Doelman, G. Hek, and J. D. M. Rademacher, *Rise and fall of periodic patterns for a generalized Klausmeier-Gray–Scott model*, J. Nonlinear Sci., 23 (2013), pp. 39–95.
[41] L. Sewalt and A. Doelman, *Spatially periodic multipulse patterns in a generalized Klausmeier–Gray–Scott model*, SIAM J. Appl. Dyn. Syst., 16 (2017), pp. 1113–1163, https://doi.org/10.1137/16M1078756.
[42] J. A. Sherratt, *Wavefront propagation in a competition equation with a new motility term modelling contact inhibition between cell populations*, Proc. R. Soc. Lond. Ser. A Math. Phys. Eng. Sci., 456 (2000), pp. 2365–2386.
[43] M. J. Ward and J. Wei, *Hopf bifurcations and oscillatory instabilities of spike solutions for the one-dimensional Gierer-Meinhardt model*, J. Nonlinear Sci., 13 (2003), pp. 209–264.
[44] W. Chen and M. J. Ward, *Oscillatory instabilities and dynamics of multi-spike patterns for the one-dimensional Gray-Scott model*, European J. Appl. Math., 20 (2009), pp. 187–214.
[45] J. M. Alexander, J. M. Diez, and J. M. Levine, *Novel competitors shape species responses to climate change*, Nature, 525 (2015), pp. 515–518.
[46] C. Damgaard, *Plant competition experiments: Testing hypotheses and estimating the probability of coexistence*, Ecology, 79 (1998), pp. 1760–1767.
[47] P. Gandhi, S. Bonetti, S. Iams, A. Porporato, and M. Silber, *A fast-slow model of banded vegetation pattern formation in drylands*, Phys. D, 410 (2020), 132534.